FIG. 2. **VPA induced HMGB1 release from macrophages.** RAW-blue cells were incubated with VPA (5 mM), LPS (100 ng/mL), and TNF-α (20 ng/mL) for 24 h (A). RAW-blue cells were incubated with VPA (5 mM) for 3, 6, 18, and 24 h (B). HMGB1 levels in supernatants were analyzed by ELISA (A and B). Translocation of HMGB1 in response to VPA (5 mM), LPS (100 ng/mL), and TNF-α (20 ng/mL) 24 h was analyzed by immunofluorescence assay (C). Cell viability was evaluated by LDH assay (D). Caspase 3/7 activity in the cells was analyzed by using a detection kit (E). Levels of *HMGB1* mRNA expresion were analyzed by real-time PCR and are shown as relative expression normalized by the levels of a housekeeping gene (*β-actin*) mRNA (F) (n = 3 ± SD, *P < 0.05 vs. control, **P < 0.01 vs. control). RAW-Blue cells were pre-incubated with Brefeldin A (50–500 ng/ml) for 3 h and were then treated with VPA (5 mM) and LPS (100 ng/ml) for 24 h. The levels of HMGB1 and IL-6 in culture media were determined by ELISA (H). (n = 3 ± S.D. **P < 0.01 vs. VPA and LPS).

and TNF-α by stimulations with LPS and VPA. Stimulation with VPA for 24 h increased steady-state levels of HMGB1 mRNA. However, LPS did not induce HMGB1 mRNA expression at a concentration of 100 ng/mL (Fig. 2G). High-mobility group box 1 mRNA levels also did not increase in RAW-blue cells primed with VPA and then stimulated with TNF-α. On the other hand, LPS strongly induced mRNA expression of TNF-α in RAW-blue cells (Fig. 2G). However, VPA did not induce its expression. These results suggest that HMGB1 release by stimulation with VPA due not to cell lysis or injury but to an active process that is not dependent on increase in gene expression and mRNA induction of HMGB1 by VPA is not due to activation of NF-κB. We also examined the effect of brefeldin A, a blocker of membrane export of proteins out of the endoplasmic reticulum, on release of HMGB1 induced by VPA and LPS. As shown in Figure 2H, the release of HMGB1 stimulated with VPA and LPS did not suppress by addition of brefeldin A, although the release of IL-6 stimulated with these stimulants suppressed with it at a concentration of 50 ng/ml. These results suggest that HMGB1

release with VPA and LPS were not due to the conventional secretory pathway.

ERK kinase may play a role in VPA-induced HMGB1 release

To clarify the mechanism by which VPA induces the release of HMGB1, we examined whether MAP kinases mediate VPA-induced HMGB1 release. Treatment of macrophages with VPA for 0.5 or 24 h activated phosphorylation of ERK (Fig. 3A). However, VPA did not induce phosphorylation of JNK and p38. In contrast, LPS induced phosphorylation of ERK, JNK, and p38. Inhibition of ERK with PD98059 suppressed VPA-induced ERK phosphorylation and HMGB1 release by macrophages (Fig. 3B and Supplemental Digital Content 5, at http://links.lww.com/SHK/A90). Valproic acid also induced NF-κB activation in macrophages (Fig. 3C), and it was inhibited by treatment with PD98059 (Fig. 3D). These findings suggest that VPA stimulates the release of HMGB1 from activated macrophages via ERK MAP kinase and NF-κB signaling. A recent study showed that acetylation of cytosolic HMGB1 triggers its exocytosis from monocytic cells (21).
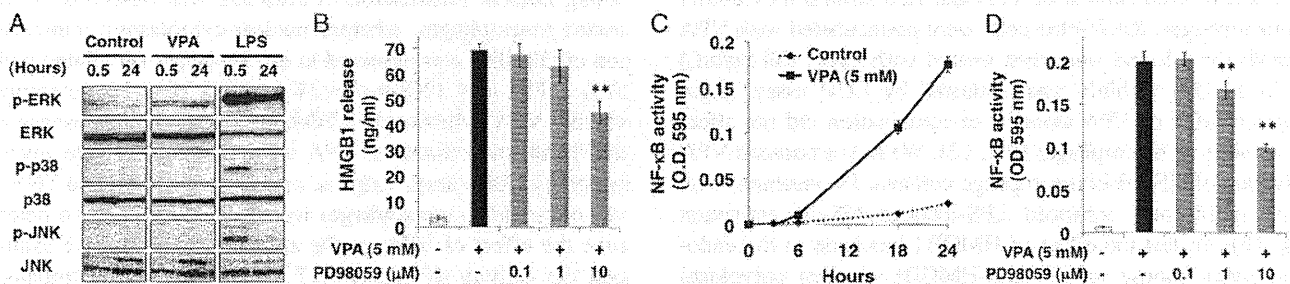

FIG. 3. **ERK kinase mediates VPA-induced HMGB1 release.** RAW-blue cells were incubated with VPA (5 mM) and LPS (100 ng/mL) for 0.5 to 24 h. Phosphorylation of p38MAPK, ERK1/2, and JNK was assayed by Western blot analysis (A). RAW-blue cells were incubated with VPA (5 mM) and PD98059 (0.1–10 μM) for 24 h. The levels of HMGB1 in culture supernatants were analyzed by ELISA (B). RAW-blue cells were incubated with VPA (5 mM) for 3, 6, 18, and 24 h (C). RAW-blue cells were incubated with VPA (5 mM) and PD98059 (0.1–10 μM) for 24 h (D). The levels of NF-κB activation were analyzed by reporter assay, as described in Materials and Methods (C and D) (n = 3 ± SD, **P < 0.01 vs. VPA).
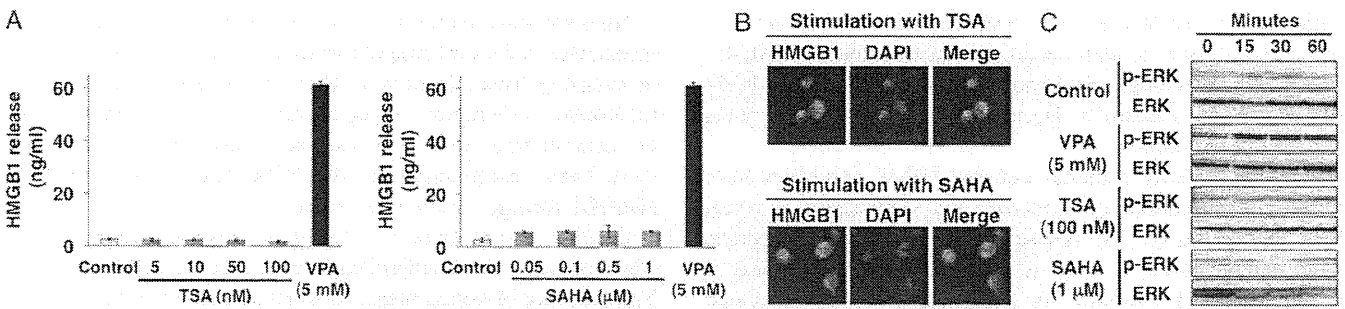
FIG. 4. **Histone deacetylases do not mediate the effects of VPA on HMGB1 release.** RAW-blue cells were incubated in histone deacetylase inhibitors TSA (5–100 nM) or SAHA (0.05–1 μM) for 24 h. The levels of HMGB1 in supernatants were evaluated by ELISA (A). Translocation of HMGB1 in response to TSA (100 nM) and SAHA (1 μM) for 24 h was analyzed by immunofluorescence assay (B). RAW-blue cells were incubated with VPA (5 mM), TSA (100 nM), and SAHA (1 μM) for 0 to 1 h. Phosphorylation of ERK1/2 was assayed by Western blot analysis (C) (n = 3 ± SD).

HDACs do not mediate the effects of VPA on HMGB1 release

Therefore, we examined the effects of TSA and SAHA, inhibitors of HDAC, on VPA-induced HMGB1 release in macrophage cultures. Trichostatin A and SAHA did not induce HMGB1 release from macrophages (Fig. 4A). In addition, HMGB1 was retained in nuclear regions, and the levels of HMGB1 in the cytoplasmic region were not increased after treatment with TSA and SAHA (Fig. 4B). Furthermore, TSA and SAHA did not activate phosphorylation of ERK, although VPA activated phosphorylation of ERK in the same conditions (Fig. 4C). These results suggest that VPA-induced HMGB1 release is not due to its inhibitory effect on HDACs.

VPA activates GABA signaling

Valproic acid exerts its antiepileptic effect principally by elevating GABA concentration in the brain (22, 23). Therefore, we next examined whether VPA increases GABA concentration in macrophage cultures. RAW-blue cells were stimulated with 5 mM of VPA for 24 h. γ-Aminobutyric acid levels in the cytoplasm and supernatants were analyzed by ELISA. Valproic acid induced GABA release into media (Figures 1A and B, Supplemental Digital Content 1, at http://links.lww.com/SHK/A85, and Supplemental Digital Content 2, at http://links.lww.com/SHK/A86). RAW cells were stimulated with VPA (5 mM) for 24 h. γ-Aminobutyric acid levels in supernatants (A) and cytoplasms (B) were analyzed by ELISA (n = 3 ± SD). We then confirmed that GABA release from macrophages acts on macrophages through a paracrine pathway and induces HMGB1 release. We examined the effect of GABA on HMGB1 release in macrophages. γ-Aminobutyric

acid at concentrations of 1 to 1,000 μM did not activate the release of HMGB1 (Figures 2A and B, Supplemental Digital Content 3, at http://links.lww.com/SHK/A87, and Supplemental Digital Content 4, at http://links.lww.com/SHK/A88). RAW cells were stimulated with various concentrations (1–1,000 μM) of GABA for 24 h. High-mobility group box 1 levels in supernatants were analyzed by ELISA (A). Cell viability was evaluated by LDH assay (B) (n = 3 ± SD). These findings suggest that GABA did not mediate HMGB1 release induced by VPA.

Next, we examined whether VPA induces expression of GABA receptors in macrophages. RAW cells were stimulated with 5 mM of VPA for 24 h, and expression of $GABA_A$ receptor subunits in murine macrophages was investigated by quantitative RT-PCR. Among the α and β subunits, the $β_2$ subunit was expressed in macrophages (Fig. 5A). Expression of the $α_1$ and $α_3$ subunits of the $GABA_A$ receptor was induced by stimulation with 5 mM of VPA (Fig. 5A). Expression of $α_2$, $α_4$, $α_5$, and $β_1$ was not detected in macrophages with or without VPA stimulation (Fig. 5A). Picrotoxin, a $GABA_A$ receptor antagonist, inhibited VPA-induced HMGB1 release at a concentration of 0.5 μM (Fig. 5B). Picrotoxin also inhibited the activation of ERK phosphorylation by stimulation with VPA in macrophages (Fig. 5C). These results suggest that VPA induces HMGB1 release in macrophages in part through activation of $GABA_A$ receptors and ERK kinase.

DISCUSSION

In the present study, we demonstrated that VPA significantly augmented the proinflammatory response induced by
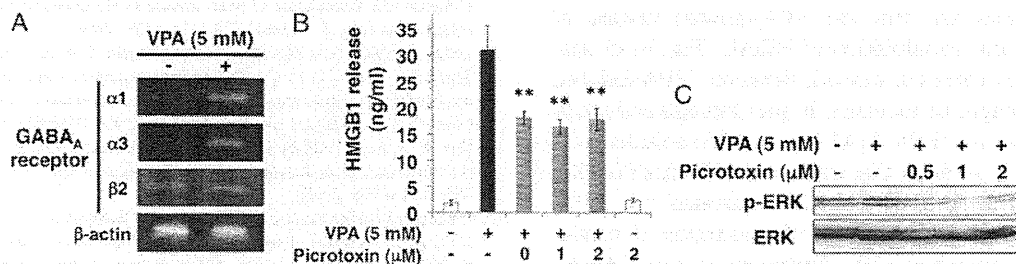

FIG. 5. **Valproic acid induced HMGB1 release by activating the $GABA_A$ receptor.** RAW-blue cells were stimulated with VPA (5 mM) for 24 h. Expression of $GABA_A$ receptor mRNA was analyzed by RT-PCR (A).RAW-blue cells were incubated with VPA (5 mM) in the presence or absence of picrotoxin (2 μM) for 24 h. The levels of HMGB1 in supernatants were analyzed by ELISA (B). Phosphorylation of ERK1/2 was detected by Western blot analysis (C) (n = 3 ± SD, **P < 0.01 vs. VPA).

LPS both *in vivo* and *in vitro*. Valproic acid reduced survival in a mouse model of lethal endotoxemia by inducing HMGB1 release. Pharmacologic data show that VPA induces HMGB1 release through a pathway that might include GABA receptors and ERK MAP kinase.

A previous study demonstrated that HDAC inhibitors have broad anti-inflammatory properties via suppression of cytokine production (6, 24). These anti-inflammatory properties were demonstrated *in vitro* by inhibition of the secretion of proinflammatory cytokines in LPS- and cytokine-stimulated peripheral blood mononuclear cells (PBMCs) and in macrophages (6). Histone deacetylase inhibitors reduced circulating cytokine concentrations during endotoxemia in mice (25). Histone deacetylase inhibitors, by increasing the levels of histone acetylation, can lead to a local alteration in the structure of chromatin, which facilitates gene-specific repression of transcription. Therefore, HDAC inhibition is a relevant mechanism mediating anti-inflammatory effects.

How do HDACs and HDAC inhibitors regulate inflammation? Histone deacetylases were originally identified as enzymes that modify acetylation of histone proteins, thereby regulating gene expression. However, subsequent research has identified many other targets of acetylation, and acetylation of nonhistone proteins regulates a variety of other cell signaling pathways, including inflammation. Thus, at least three distinct pathways may exist for HDAC regulation of inflammation. First, HDACs might regulate gene expression of inflammatory mediators through modification of histone proteins. Second, HDACs might regulate transcription factors such as NF-κB that transactivate proinflammatory genes. Third, HDACs directly modify members of the mitogen-activated protein kinase (MAPK) pathway, such as MAPK phosphatase-1 (MKP-1), which in turn modulate transcription factors controlling innate immune responses (12).

Valproic acid is an HDAC inhibitor of the class of short-chain fatty acids, and it exhibited anti-inflammatory effects through histone hyperacetylation (16, 26). On the other hand, several mechanisms are known to promote the relocation of HMGB1 from the nucleus to cytoplasm, including the acetylation (21, 27) and phosphorylation (28) of HMGB1 and the destabilized association of HMGB1 with chromatin or a nuclear import protein (28). High-mobility group box 1 has been reported to be a substrate of histone acetylase, and it has been shown that HDAC inhibitors induce the relocation of HMGB1 from the nucleus to cytoplasm (21, 27). In this study, we demonstrated that VPA induced HMGB1 release in macrophage cultures and that the VPA-induced release of HMGB1 was not due to inhibition of HDAC (Fig. 4) or acetylation of HMGB1 (data not shown). However, VPA-induced HMGB1 release might be mediated in part through activation of GABA receptors and ERK MAP kinase. This conclusion is strengthened by our findings that inhibitors of ERK or GABA receptors abolished HMGB1 release stimulated by VPA. Phosphorylation of ERK is important for secretion of insulin (29) and various cytokines (30). Furthermore, the GABA$_A$ receptor regulates the phosphorylation of ERK. Therefore, our studies support the theory that MAPK signaling and GABA signaling mediate VPA activation of HMGB1 release.

High-mobility group box 1 is either secreted from activated monocytes and macrophages through secretory lysosomes (31) or passively leaked from cells when the integrity of the plasma membrane is disrupted during necrosis (32, 33). In this study, we demonstrated that VPA does not cause necrosis or apoptosis. These results suggested that VPA induced the release of HMGB1 through active exocytosis.

Gingival overgrowth is a common adverse effect of the administration of an antiepileptic drug such as VPA (19, 34). The presence of dental plaque is often associated with gingival overgrowth (35). Morphological changes in the gingiva lead to the retention of dental plaque. Bacterial components, such as LPS and lipoprotein, in dental plaque can be recognized by host cell Toll-like receptors and play an important role in the inflammatory response in periodontal tissue. Higher levels of HMGB1 were shown to be present in gingival crevicular fluid from periodontal patients (36). High-mobility group box 1 potentiates the action of LPS (37), and thus release of HMGB1 induced by VPA may exaggerate the outcome of bacterial insult in periodontal tissue.

REFERENCES

1. Wang H, Bloom O, Zhang M, Vishnubhakat JM, Ombrellino M, Che J, Frazier A, Yang H, Ivanova S, Borovikova L, et al.: HMG-1 as a late mediator of endotoxin lethality in mice. *Science* 285:248–251, 1999.
2. Gotfryd K, Skladchikova G, Lepekhin EA, Berezin V, Bock E, Walmod PS: Cell type-specific anti-cancer properties of valproic acid: independent effects on HDAC activity and Erk1/2 phosphorylation. *BMC Cancer* 10:383, 2010.
3. Zhu K, Qu D, Sakamoto T, Fukasawa I, Hayashi M, Inaba N: Telomerase expression and cell proliferation in ovarian cancer cells induced by histone deacetylase inhibitors. *Arch Gynecol Obstet* 277:15–19, 2008.
4. Duenas-Gonzalez A, Candelaria M, Perez-Plascencia C, Perez-Cardenas E, de la Cruz-Hernandez E, Herrera LA: Valproic acid as epigenetic cancer drug: preclinical, clinical and transcriptional effects on solid tumors. *Cancer Treat Rev* 34:206–222, 2008.
5. Hrzenjak A, Moinfar F, Kremser ML, Strohmeier B, Petru E, Zatloukal K, Denk H: Histone deacetylase inhibitor vorinostat suppresses the growth of uterine sarcomas *in vitro* and *in vivo*. *Mol Cancer* 9:49, 2010.
6. Halili MA, Andrews MR, Labzin LI, Schroder K, Matthias G, Cao C, Lovelace E, Reid RC, Le GT, Hume DA, et al.: Differential effects of selective HDAC inhibitors on macrophage inflammatory responses to the Toll-like receptor 4 agonist LPS. *J Leukoc Biol* 87:1103–1114, 2010.
7. Faraco G, Pittelli M, Cavone L, Fossati S, Porcu M, Mascagni P, Fossati G, Moroni F, Chiarugi A: Histone deacetylase (HDAC) inhibitors reduce the glial inflammatory response *in vitro* and *in vivo*. *Neurobiol Dis* 36:269–279, 2009.
8. Han SB, Lee JK: Anti-inflammatory effect of trichostatin-A on murine bone marrow-derived macrophages. *Arch Pharm Res* 32:613–624, 2009.
9. Kim HJ, Rowe M, Ren M, Hong JS, Chen PS, Chuang DM: Histone deacetylase inhibitors exhibit anti-inflammatory and neuroprotective effects in a rat permanent ischemic model of stroke: multiple mechanisms of action. *J Pharmacol Exp Ther* 321:892–901, 2007.
10. Reilly CM, Mishra N, Miller JM, Joshi D, Ruiz P, Richon VM, Marks PA, Gilkeson GS: Modulation of renal disease in MRL/lpr mice by suberoylanilide hydroxamic acid. *J Immunol* 173:4171–4178, 2004.
11. Leoni F, Zaliani A, Bertolini G, Porro G, Pagani P, Pozzi P, Dona G, Fossati G, Sozzani S, Azam T, et al.: The antitumor histone deacetylase inhibitor suberoylanilide hydroxamic acid exhibits antiinflammatory properties via suppression of cytokines. *Proc Natl Acad Sci U S A* 99:2995–3000, 2002.
12. Cao W, Bao C, Padalko E, Lowenstein CJ: Acetylation of mitogen-activated protein kinase phosphatase-1 inhibits Toll-like receptor signaling. *J Exp Med* 205:1491–1503, 2008.
13. Gottlicher M, Minucci S, Zhu P, Kramer OH, Schimpf A, Giavara S, Sleeman JP, Lo Coco F, Nervi C, Pelicci PG, et al.: Valproic acid defines a novel class of HDAC inhibitors inducing differentiation of transformed cells. *EMBO J* 20:6969–6978, 2001.
14. Herranz JL, Armijo JA, Arteaga R: Clinical side effects of phenobarbital, primidone, phenytoin, carbamazepine, and valproate during monotherapy in children. *Epilepsia* 29:794–804, 1988.

15. Blaheta RA, Cinatl J Jr: Anti-tumor mechanisms of valproate: a novel role for an old drug. *Med Res Rev* 22:492–511, 2002.
16. Ichiyama T, Okada K, Lipton JM, Matsubara T, Hayashi T, Furukawa S: Sodium valproate inhibits production of TNF-alpha and IL-6 and activation of NF-kappaB. *Brain Res* 857:246–251, 2000.
17. Garnier R, Boudignat O, Fournier PE: Valproate poisoning. *Lancet* 2:97, 1982.
18. El-Mowafy AM, Abdel-Dayem MA, Abdel-Aziz A, El-Azab MF, Said SA: Eicosapentaenoic acid ablates valproate-induced liver oxidative stress and cellular derangement without altering its clearance rate: dynamic synergy and therapeutic utility. *Biochim Biophys Acta* 1811:460–467, 2011.
19. Anderson HH, Rapley JW, Williams DR: Gingival overgrowth with valproic acid: a case report. *ASDC J Dent Child* 64:294–297, 1997.
20. Galanos C, Roppel J, Weckesser J, Rietschel ET, Mayer H: Biological activities of lipopolysaccharides and lipid A from Rhodospirillaceae. *Infect Immun* 16:407–412, 1977.
21. Bonaldi T, Talamo F, Scaffidi P, Ferrera D, Porto A, Bachi A, Rubartelli A, Agresti A, Bianchi ME: Monocytic cells hyperacetylate chromatin protein HMGB1 to redirect it towards secretion. *EMBO J* 22:5551–5560, 2003.
22. Nau H, Loscher W: Valproic acid: brain and plasma levels of the drug and its metabolites, anticonvulsant effects and gamma-aminobutyric acid (GABA) metabolism in the mouse. *J Pharmacol Exp Ther* 220:654–659, 1982.
23. Guidotti A, Auta J, Chen Y, Davis JM, Dong E, Gavin DP, Grayson DR, Matrisciano F, Pinna G, Satta R, et al.: Epigenetic GABAergic targets in schizophrenia and bipolar disorder. *Neuropharmacology* 60:1007–1016, 2011.
24. Halili MA, Andrews MR, Sweet MJ, Fairlie DP: Histone deacetylase inhibitors in inflammatory disease. *Curr Top Med Chem* 9:309–319, 2009.
25. Roger T, Lugrin J, Le Roy D, Goy G, Mombelli M, Koessler T, Ding XC, Chanson AL, Knaup Reymond M, Miconnet I, et al.: Histone deacetylase inhibitors impair innate immune responses to Toll-like receptor agonists and to infection. *Blood* 117:1205–1217, 2011.
26. Zhang Z, Zhang ZY, Fauser U, Schluesener HJ: Valproic acid attenuates inflammation in experimental autoimmune neuritis. *Cell Mol Life Sci* 65:4055–4065, 2008.
27. Carneiro VC, de Moraes Maciel R, de Abreu da Silva IC, da Costa RF, Paiva CN, Bozza MT, Fantappie MR: The extracellular release of *Schistosoma mansoni* HMGB1 nuclear protein is mediated by acetylation. *Biochem Biophys Res Commun* 390:1245–1249, 2009.
28. Youn JH, Shin JS: Nucleocytoplasmic shuttling of HMGB1 is regulated by phosphorylation that redirects it toward secretion. *J Immunol* 177:7889–7897, 2006.
29. Persaud SJ, Wheeler-Jones CP, Jones PM: The mitogen-activated protein kinase pathway in rat islets of Langerhans: studies on the regulation of insulin secretion. *Biochem J* 313:119–124, 1996.
30. Kawahara K, Biswas KK, Unoshima M, Ito T, Kikuchi K, Morimoto Y, Iwata M, Tancharoen S, Oyama Y, Takenouchi K, et al.: C-reactive protein induces high-mobility group box-1 protein release through activation of p38MAPK in macrophage RAW264.7 cells. *Cardiovasc Pathol* 17:129–138, 2008.
31. Gardella S, Andrei C, Ferrera D, Lotti LV, Torrisi MR, Bianchi ME, Rubartelli A: The nuclear protein HMGB1 is secreted by monocytes via a non-classical, vesicle-mediated secretory pathway. *EMBO Rep* 3:995–1001, 2002.
32. Scaffidi P, Misteli T, Bianchi ME: Release of chromatin protein HMGB1 by necrotic cells triggers inflammation. *Nature* 418:191–195, 2002.
33. Bianchi ME, Manfredi AA: High-mobility group box 1 (HMGB1) protein at the crossroads between innate and adaptive immunity. *Immunol Rev* 220:35–46, 2007.
34. Seymour RA, Smith DG, Turnbull DN: The effects of phenytoin and sodium valproate on the periodontal health of adult epileptic patients. *J Clin Periodontol* 12:413–419, 1985.
35. Seymour RA, Ellis JS, Thomason JM: Risk factors for drug-induced gingival overgrowth. *J Clin Periodontol* 27:217–223, 2000.
36. Morimoto Y, Kawahara KI, Tancharoen S, Kikuchi K, Matsuyama T, Hashiguchi T, Izumi Y, Maruyama I: Tumor necrosis factor-alpha stimulates gingival epithelial cells to release high mobility-group box 1. *J Periodontal Res* 43:76–83, 2008.
37. Qin YH, Dai SM, Tang GS, Zhang J, Ren D, Wang ZW, Shen Q: HMGB1 enhances the proinflammatory activity of lipopolysaccharide by promoting the phosphorylation of MAPK p38 through receptor for advanced glycation end products. *J Immunol* 183:6244–6250, 2009.

Complete Pulp Regeneration After Pulpectomy by Transplantation of CD105+ Stem Cells with Stromal Cell-Derived Factor-1

Koichiro Iohara, Ph.D.,[1] Kiyomi Imabayashi, Ph.D.,[1] Ryo Ishizaka, D.D.S.,[1,2] Atsushi Watanabe, Ph.D.,[3] Junichi Nabekura, Ph.D.,[4] Masataka Ito, Ph.D.,[5] Kenji Matsushita, Ph.D.,[1] Hiroshi Nakamura, Ph.D.,[6] and Misako Nakashima, Ph.D.[1]

Loss of pulp due to caries and pulpitis leads to loss of teeth and reduced quality of life. Thus, there is an unmet need for regeneration of pulp. A promising approach is stem cell therapy. Autologous pulp stem/progenitor (CD105+) cells were transplanted into a root canal with stromal cell-derived factor-1 (SDF-1) after pulpectomy in mature teeth with complete apical closure in dogs. The root canal was successfully filled with regenerated pulp including nerves and vasculature by day 14, followed by new dentin formation along the dentinal wall. The newly regenerated tissue was significantly larger in the transplantation of pulp CD105+ cells with SDF-1 compared with those of adipose CD105+ cells with SDF-1 or unfractionated total pulp cells with SDF-1. The pulp CD105+ cells highly expressed angiogenic/neurotrophic factors compared with other cells and localized in the vicinity of newly formed capillaries after transplantation, demonstrating its potent trophic effects on neovascularization. Two-dimensional electrophoretic analyses and real-time reverse transcription–polymerase chain reaction analyses demonstrated that the qualitative and quantitative protein and mRNA expression patterns of the regenerated pulp were similar to those of normal pulp. Thus, this novel stem cell therapy is the first demonstration of complete pulp regeneration, implying novel treatment to preserve and save teeth.

Introduction

DENTAL PULP has many functions, and it is essential for longevity of teeth and quality of life. The long-term goal of endodontic treatment after deep caries and/or pulp inflammation is the conservation and restoration of teeth including dental pulp. A promising approach for it is stem-cell-based therapy to regenerate the dentin-pulp complex for the conservation and total restoration of structure and function.[1] The regeneration and tissue engineering of pulp is based on morphogens and growth factors, responding stem/progenitor cells, and the extracellular matrix scaffold.[2] The regeneration of dental pulp in immature teeth with incomplete apical closure has been reported using fibrin in the blood clot or collagen.[3,4] However, there have been no reports concerning total pulp regeneration in mature teeth with complete apical closure by stem/progenitor cell therapy. There is an intimate association of innervation with vasculature of the dental pulp. Angiogenesis/ vasculogenesis and neurogenesis are critical for total functional pulp regeneration. The type III receptor of the transforming growth factor-β receptor family cell surface antigen CD105 (endoglin) was selected on the basis of its wide expression on mesenchymal stem cells (MSCs).[5] The stromal cell-derived factor-1 (SDF-1)/CXCR4 axis is present and functional in MSC populations.[6,7] CD105+ stem/progenitor cells from human pulp tissue containing CXCR4-positive cells demonstrated angiogenic/vasculogenic and neurogenic potential.[8] Endothelial cells release SDF-1 under hypoxic conditions and promote cell survival and neovascularization by recruitment and perivascular retention of CXCR4-positive bone marrow-derived cells.[9,10] Therefore, in this study, autologous pulp CD105+ cells were transplanted with SDF-1 in a collagen scaffold into the root canal of mature teeth induced complete apical closure after pulpectomy, in dogs. Thus, we demonstrate for the first time complete pulp regeneration in the root canal, by protein profiles and mRNA expression patterns.

[1]Department of Dental Regenerative Medicine, Center of Advanced Medicine for Dental and Oral Diseases, National Center for Geriatrics and Gerontology, Research Institute, Obu, Aichi, Japan.
[2]Department of Pediatric Dentistry, School of Dentistry, Aichi-gakuin University, Nagoya, Aichi, Japan.
[3]Department of Cognitive Brain Science, National Center for Geriatrics and Gerontology, Research Institute, Obu, Aichi, Japan.
[4]Department of Developmental Physiology, National Institute for Physiological Sciences, Okazaki, Aichi, Japan.
[5]Department of Developmental Anatomy and Regenerative Medicine, National Defense Medical College, Tokorozawa, Saitama, Japan.
[6]Department of Endodontology, School of Dentistry, Aichigakuin University, Nagoya, Aichi, Japan.

Materials and Methods

Cell isolation

Dental pulp cells were separated from pulp tissues of maxillary teeth in dogs as previously described.[11] Primary adipose cells were also separated from the adipose tissue of the same dog as a control. Those primary cells, $2-5 \times 10^5$ cells each were stained with anti-mouse IgG1 negative control (W3/25) (AbD Serotec), mouse IgG1 negative control (Phycoerythrin [PE]) (MCA928PE) (AbD Serotec), and mouse anti-human CD105 (PE) (43A3) (BioLegend), 10 μL per 10^6 cells for 90 min at 4°C, and were sorted by a flow cytometer JSAN (Bay Bioscience). Both CD105$^+$ cells and CD105$^-$ cells derived from the pulp and adipose tissue and total pulp cells without cell fractionation were cultured in EBM2 (Cambrex Bio Science) supplemented with 10 ng/mL IGF (Cambrex Bio Science), 5 ng/mL EGF (Cambrex Bio Science), and 10% FBS (Invitrogen Corporation) to maintain the cells. They were subcultured after reaching 60%–70% confluence.

The phenotype of pulp CD105$^+$ cells was further characterized by flowcytometry at the third passage of culture in comparison with adipose CD105$^+$ cells and unfractionated total pulp cells after immunolabeling with antigen surface markers (Supplementary Material; Supplementary Data are available online at www.liebertonline.com/tea). The experiments were repeated nine times.

Real-time reverse transcription-polymerase chain reaction analysis

To further characterize the phenotype of the cell populations, total RNA were extracted using Trizol (Invitrogen) from the pulp and adipose CD105$^+$ cells and total pulp cells at the third passage. The number of these cells was normalized to 5×10^4 cells in each experiment. First-strand cDNA syntheses were performed from total RNA by reverse transcription using the ReverTra Ace-α (Toyobo). Real-time reverse transcription–polymerase chain reaction (RT-PCR) amplifications were performed at 95°C for 10 s, 62°C for 15 s, and 72°C for 8 s using stem cell markers, canine *CXCR4*, *Sox2*, *Stat3*, *Bmi1*, and *Rex1* (Supplementary Table S1) labeled with Light Cycler-Fast Start DNA master SYBR Green I (Roche Diagnostics) in Light Cycler (Roche Diagnostics). The design of the oligonucleotide primers was based on published canine cDNA sequences. When canine sequences were not available, human sequences were used. To examine mRNA expression of angiogenic and neurotrophic factors, real-time RT-PCR amplifications of canine *matrix metalloproteinase-3* (*MMP-3*), *VEGF-A*, *granulocyte-monocyte colony-stimulating factor* (*GM-CSF*), *SDF-1*, *nerve growth factor* (*NGF*), *brain-derived neurotrophic factor* (*BDNF*), *Neuropeptide Y*, *Neurotrophin 3*, *E-selectin*, *VCAM 1*, *rhombotin 2*, *ECSCR*, and *SLC6A6* were also performed (Supplementary Table S1). The RT-PCR products were confirmed by sequencing based on published cDNA sequences. The expression in pulp CD105$^+$ cells and adipose CD105$^+$ cells was compared with that in total pulp cells at the third passage of culture after normalizing with β-*actin*.

Induced differentiation

The differentiation of pulp CD105$^+$ cells from the third to fifth passage, into adipogenic, angiogenic, neurogenic, and odontogenic/osteogenic lineages, was determined and compared with adipose CD105$^+$ cells and unfractionated pulp cells as previously described.[12]

Proliferation and migration assay

To determine cell proliferation in response to SDF1 (Acris), pulp CD105$^+$ cells were compared with total pulp cells and adipose CD105$^+$ cells at fourth passage at the 10^3 cells per 96 well in EBM2 supplemented with 0.2% bovine serum albumin (Sigma) and SDF-1 (50 ng/mL). Ten microliters of Tetracolor one® (Seikagaku Kogyo) was added to the 96-well plate, and cell numbers were measured at 2, 12, 24, and 36 h of culture using a spectrophotometer at 450 nm absorbance. Wells without cells served as negative controls.

To examine migration activity of pulp CD105$^+$ cells by SDF-1, horizontal chemotaxis assay was performed and compared with total pulp cells and adipose CD105$^+$ cells. The TAXIScan-FL (Effector Cell Institute) was used to detect real-time horizontal chemotaxis of cells. The TAXIScan-FL consists of an etched silicon substrate and a flat glass plate, both of which form two compartments with a 6 μm deep microchannel. Each cell fraction (1 μL of 10^5cells/mL) was placed into the single hole with which the device is held together with a stainless steel holder, and 1 μL of 10 ng/μL of SDF-1 was placed into the contra-hole. The video images of cell migration were taken for 6 h.

In vivo transplantation studies

An experimental model of whole pulp removal and transplantation of cell populations for regeneration was established in the permanent teeth in dogs to achieve complete apical closure (Narc). The whole pulp removal was carried out in both sides of upper second incisors and lower third incisors under intravenously administered sodium pentobarbital (Schering-Plough) followed by enlargement of apical foramen, 0.7 mm in width using #70 K-file (MANI). Autologous transplantation of the pulp CD105$^+$ cells, adipose CD105$^+$ cells, or total pulp cells, 1×10^6cells in each, from the third to fourth passage, after DiI labeling was performed with collagen TE, a mixture of collagen type I and type III (Nitta Gelatin) in the lower part of the root canals. The upper part of the root canals was further filled with SDF-1 at the final concentration of 15 ng/μL, with collagen TE. The cavity was sealed with zinc phosphate cement (Elite Cement, GC) and composite resin (Clearfil FII) after treatment with a bonding agent (Clearfil Mega Bond). Sixty teeth from 15 dogs were used. Ten teeth transplanted with pulp CD105$^+$ cells with SDF-1, 5 teeth transplanted with adipose CD105$^+$ cells with SDF-1, 5 teeth transplanted with total pulp cells with SDF-1, 5 teeth with SDF-1 only without cells, 5 teeth with pulp CD105$^+$ cells only without SDF-1, and 5 teeth with a scaffold only without cells were harvested for histology after 14 days. Six teeth transplanted with pulp CD105$^+$ cells with SDF-1 were harvested for two-dimensional electrophoretic analyses after 28 days. Four teeth each transplanted with pulp CD105$^+$ cells with SDF-1, adipose CD105$^+$ cells with SDF-1, and total pulp cells with SDF-1 were harvested after 90 days, respectively. Seven normal teeth without any operation were used as control. For morphological analyses, they were fixed in 4% paraformaldehyde (Nakarai Tesque) at 4°C overnight and embedded in paraffin wax (Sigma) after demineralization with 10% formic acid. The paraffin sections
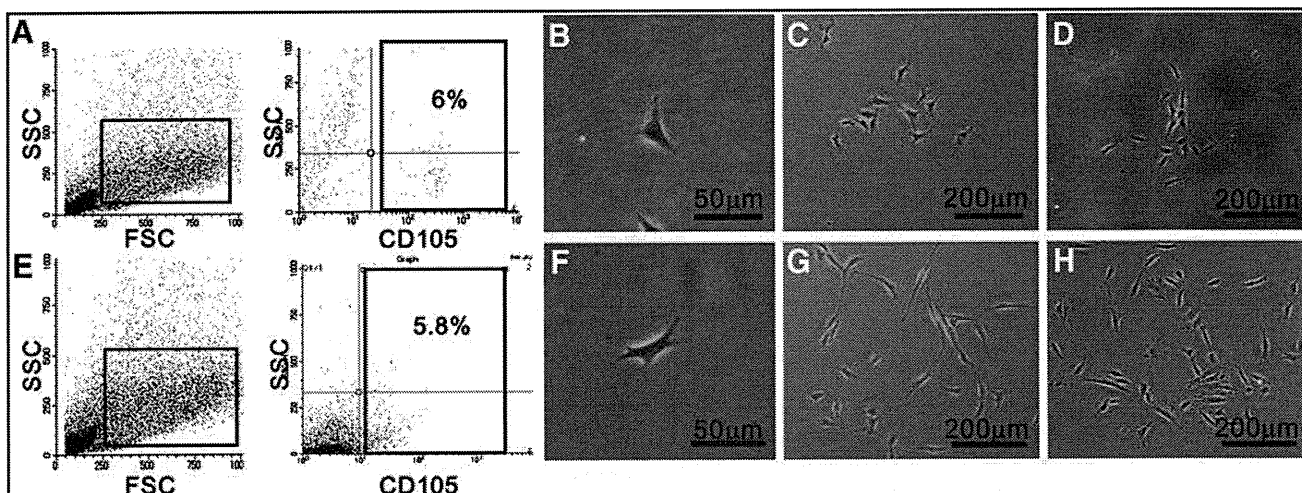
FIG. 1. Isolation of CD105$^+$ cells from adult canine dental pulp and adipose tissue. **(A)** The two panels show flow cytometry profiles of forward scatter (FSC) and side scatter (SSC) (left), and CD105 and SSC expression (right) on the dental pulp tissue. CD105$^+$ cells represented 6% of the total. **(B)** Primary pulp CD105$^+$ cell culture on day 3. **(C)** Primary pulp CD105$^+$ cell culture on day 10. **(D)** Primary total pulp cells on day 10. **(E)** The two panels show flow cytometry profiles of FSC and SSC (left), and CD105 and SSC expression (right) on the adipose tissue. CD105$^+$ cells represented 5.8% of the total. **(F)** Primary adipose CD105$^+$ cell culture on day 3. **(G)** Primary adipose CD105$^+$ cell culture on day 10. **(H)** Primary total adipose cells on day 10. The experiments were repeated nine times, and one represented experiment is presented. Color images available online at www.liebertonline.com/tea

(5 μm in thickness) were morphologically examined after staining with hematoxylin and eosin (HE).

All animal experiments were conducted using the strict guidelines of the Animal Protocol Committees and DNA Safety Programs both in National Center for Geriatrics and Gerontology and Aichigakuin University.

For vascular staining, 5-μm-thick paraffin sections stained with Fluorescein Griffonia (Bandeiraea) Simplicifolia Lectin 1/fluorescein-galanthus nivalis (snowdrop) lectin (20 μg/mL; Vector laboratories) for 15 min a fluorescence microscope BIOREVO, BZ-9000 (KEYENCE) were used.

For whole mount staining of vascular structure, the regenerated tissue and normal pulp tissue were dissected from teeth on day 14 and fixed in 4% paraformaldehyde for 45 min. The tissue was treated with 0.3% Triton X in phosphate-buffered saline, blocked, and stained with isolectin GS-IB4 from Griffonia simplicifolia, Alexa Fluor 488 conjugate (1:500) for 12 h at 4°C overnight. Neovascularization and engraftment of the transplanted cells into the root canal was examined by two-photon microscopy using FV1000MPE (Olympus) instrument. Three-dimensional structures were reconstructed by FV10-ASW software.

For neuronal staining, 5-μm-thick paraffin sections were incubated for 15 min with 0.3% Triton X-100 (Sigma Chemical). After incubation with 2.0% normal goat serum to block non-specific binding, they were incubated with goat anti-human PGP9.5 (Ultra Clone) (1:10000) at 4°C overnight. After three washes in phosphate-buffered saline, bound antibodies were reacted with biotinylated goat anti-rabbit IgG secondary antibody (Vector) (1:200) for 1 h at room temperature. The sections were also developed with the ABC reagent (Vector Laboratories), using the DAB chromogen for 10 min.

Relative amounts of regenerative pulp tissue 14 days after transplantation were examined in each sample by capturing video images of the histological preparations on the binoc-

ular microscopy (Leica, M 205 FA). Three sections at 150-μm intervals for each tooth from a total of 5 teeth each transplanted with pulp CD105$^+$ cells with SDF-1, adipose CD105$^+$ cells with SDF-1, total pulp cells with SDF-1, pulp CD105$^+$ cells only, SDF-1 only, and collagen TE scaffold only were examined. On-screen image outlines of newly regenerated pulp tissue and newly formed dentin were traced, and the surface area of these outlines in the root canal was determined by using Leica Application Suite software. The ratio of the regenerated area to the root canal area was calculated in three sections of each tooth, and the mean value was determined.

In vivo gene expression of odontoblastic differentiation markers, *dentin sialophosphoprotein* (*Dspp*) and *enamelysin*, in the cells lining along the root canal surface was examined by

TABLE 1. FLOW CYTOMETRIC ANALYSIS OF CELL-SURFACE MARKERS ON PULP AND ADIPOSE-DERIVED CD105$^+$ CELLS AND TOTAL PULP CELLS AT THE THIRD PASSAGE OF CULTURE

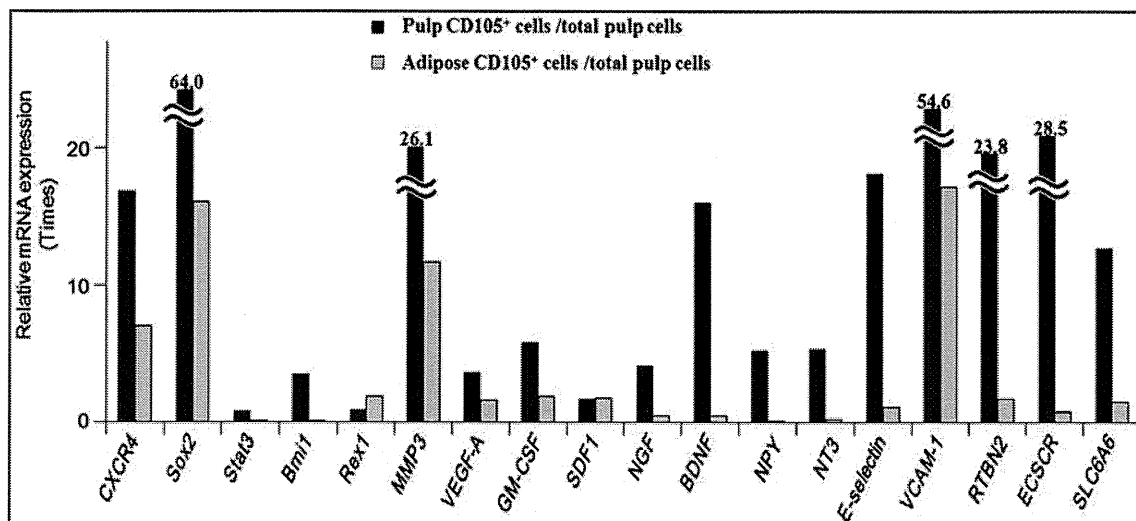|	Pulp CD105$^+$ cells	Adipose CD105$^+$ cells	Total pulp cells
CD24	1.8%	1.7%	0.3%
CD29	95.9%	90.5%	99.2%
CD31	0%	0%	0%
CD33	3.7%	0%	0.2%
CD34	45.5%	0.1%	47.1%
CD44	96.2%	92.3%	99.9%
CD73	97.2%	0.8%	22.3%
CD90	98.1%	95.6%	97.5%
CD105	98.5%	74.0%	4.6%
CD146	0.8%	0.2%	0.9%
CD150	2.3%	0.2%	0.9%
MHC class I	36.0%	80.0%	73.8%
MHC class II	0.4%	0%	0.4%
CXCR4	12.2%	5.9%	5.3%

FIG. 2. Relative mRNA expression of cytokines of vasculogenesis and neurogenesis by real-time reverse transcription-polymerase chain reaction in pulp and adipose-derived CD105$^+$ cells. The experiments were repeated four times, and one represented experiment is presented.

in situ hybridization in 5 μm-paraffin sections 90 days after transplantation of pulp CD105$^+$ cells with SDF-1. Canine cDNA of *Dspp* (183 bp) and *enamelysin* (195 bp) linearized with *Nco*I and *Spe*I, respectively, were used as anti-sense probes. The probes were constructed out of the plasmids after subcloning the PCR products using the same primers as those designed for real-time RT-PCR (Supplementary Table S1). The DIG signals were detected by TSA system (PerkinElmer).

Two-dimensional electrophoretic analyses and gene expression analyses

For two-dimensional electrophoretic analysis, the regenerated pulp-like tissue on day 28, normal pulp, and periodontal ligament were homogenized in lysis buffer (6 M urea, 1.97 M thiourea, 2% [w/v] 3-[(3-cholamidopropyl) di-methylammonio] propanesulfonate, 64.8 mM dithiothreitol [DTT], 2% [v/v] Pharmalyte) and sonicated. The supernatant was collected after being centrifuged at 15,000 rpm for 15 min at 4°C, and applied to two-dimensional electrophoresis. Isoelectric focusing (IEF) was carried out using Cool-PhoreSter 2-DE systems. IPG strips (Immobiline DryStrips, pH 4–7, 18 cm; GE) were used according to the manufacturer's instructions. IPG strips were rehydrated with rehydration solution (6 M urea, 1.97 M thiourea, 2% [v/v] TritonX-100, 13 mM DTT, 2% [v/v] Pharmalyte, 2.5 mM acetic acid, 0.0025% bromophenol blue [BPB]) overnight at 20°C. IEF was performed following a step-wise voltage incremental manner: 500 V for 2 h, 700–3000 V for 1 h, and 3500 V for 24 h. After IEF, IPG strips were incubated in an equilibration buffer (6 M urea, 32.4 mM DTT, 5 mM Tris-HCl, pH 6.8, 2% [w/v] sodium dodecyl sulfate [SDS], 0.0025% BPB, 30% [v/v] Glycerol) for 30 min. IPG strips were further equilibrated in 5 mM Tris-HCl, pH 6.8, 2% (w/v) SDS, 0.0025% BPB, 30% (v/v) Glycerol, and 243 mM iodoacetamid for 20 min. Separation in the second dimension was carried out in 12.5% SDS-PAGE gels (20 cm × 20 cm) at a constant current of 25 mA/gel for 15 min and 30 mA/gel thereafter. The gels were stained with Flamingo Fluorescent Gel Stain (Bio-Rad Laboratories) and scanned (FluoroPhorester 3000;

Anatech). The gel images were analyzed and compared with each other by using Progenesis (Nonlinear Dynamics).

Real-time RT-PCR amplifications were performed as previously described using markers for periodontal ligament, canine *axin2*, *periostin*, and *asporin*/periodontal ligament-associated protein 1 (*PLAP-1*). Collagen αI(I), *syndecan3*, and *tenascin C* were also used for comparison of regenerated tissue with normal pulp and periodontal ligament (Supplementary Table S1).

For microarray analysis, biotinylated cRNA were prepared from 250 ng of total RNA according to the standard Affymetrix protocol (Affymetrix Japan K.K.). After fragmentation, 10 μg of cRNA were hybridized for 16 h at 45°C on GeneChip Canine Genome 2.0 Array (Affymetrix) containing ~43,000 annotated sequences. GeneChips were washed and stained in the Affymetrix Fluidics Station 450, and were scanned using the Affymetrix GCS3000 scanner. The data were analyzed with Microarray Suite version 5.0 (MAS 5.0) using Affymetrix default analysis settings and global scaling as normalization method. The trimmed mean target intensity of each array was set to 500. Chips were ordered into hierarchical clusters using the Pearson centered algorithm as the distance measure, and the Average algorithm as the linkage method.

Statistical analyses

Data are reported as means ± standard deviation. *p*-Values were calculated by using the unpaired Student's *t*-test. The number of replicates in each experiment is indicated in the figure legends.

Results

Isolation and characterization of CD105$^+$ cells from pulp and adipose tissue

Flow cytometric isolation of the CD105$^+$ cells from canine adult total pulp cells (Fig. 1D) was performed using antibodies against CD105. CD105$^+$ cells isolated from total adipose cells (Fig. 1H) of the same dog and unfractionated total pulp cells were used as controls. The pulp and adipose
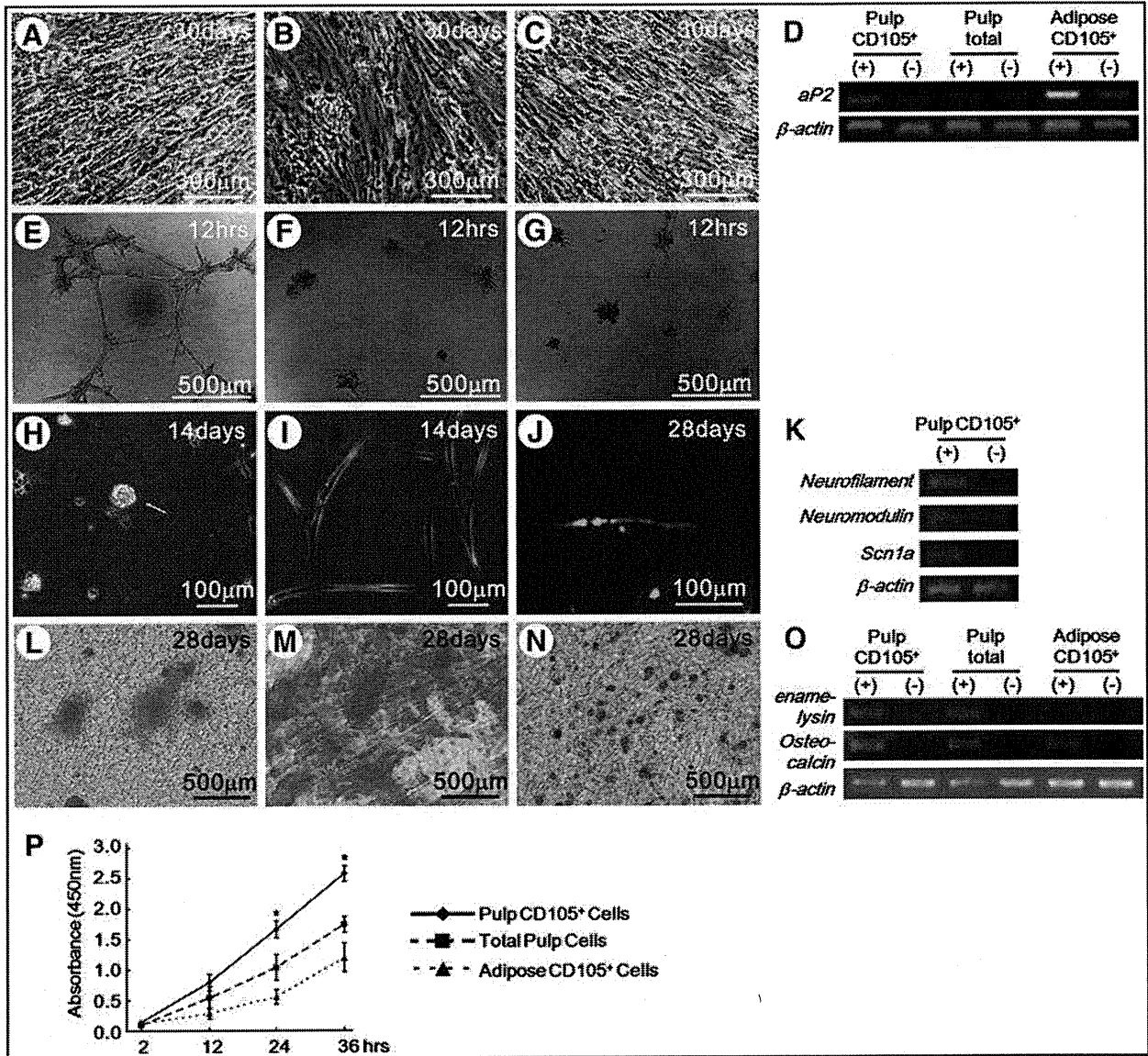
FIG. 3. Multi-lineage differentiation potential. (A–D) Adipogenic potential, (E–G) Angiogenic potential, (H, I), and Neurosphere formation. (J) Immunostaining with neurofilament. (D) Adipocyte fatty acid binding protein 2 (aP2) mRNA expression. (K) Neurofilament, neuromodulin, and sodium channel, voltage-gated, type Ia (Scn1A) mRNA expression. (L–O) Odontogenic/osteogenic potential. (O) Enamelysin and osteocalcin mRNA expression. (A–C) Oil red O staining. (L–N) Alizarin red staining. (A, E, H, J, L) Pulp CD105$^+$ cells. (B, F, I, M) Total pulp cells. (C, G, N) Adipose CD105$^+$ cells. (P) The proliferation activity of pulp CD105$^+$ cells, total pulp cells, and adipose CD105$^+$ cells with stromal cell-derived factor-1 (SDF-1). Data are expressed as means ± standard deviation of four determinations ($*p < 0.01$). The experiments were repeated thrice, and one representative experiment is presented. Color images available online at www.liebertonline.com/tea

CD105$^+$ cells represented 6% and 5.8% of total cells, respectively (Fig. 1A, E). The CD105$^+$ cells from both the pulp and the adipose tissue were stellate with long cell processes (Fig. 1B, C, F, G). The pulp CD105$^-$ cells were of varied shapes with short processes. EBM2 supplemented with IGF1, EGF, and 10% FBS maintained the phenotype of CD105$^+$ cells, demonstrating more than 98% at the sixth passage. When single CD105$^+$ cells were plated in 35 mm dishes coated with type I collagen, they formed colonies in 10 days. This demonstrates the colony formation ability of these CD 105$^+$ cells. The efficiency of attachment and growth of pulp 105$^+$, adipose CD105$^+$, and pulp CD105$^-$ cells was estimated to be 8%, 3.7%, and 1%, respectively. Limiting dilution

analysis at the third passage culture showed that the frequency of CFU in pulp CD105$^+$ cells was estimated to be 80%, whereas that in total pulp cells was 30%, and that in adipose CD105$^+$ cells was 50%.

To characterize the "stemness" of pulp CD105$^+$ cells, cell surface antigen markers were examined by flow cytometry and compared with adipose CD105$^+$ cells and total pulp cells. Pulp CD105$^+$ cells, adipose CD105$^+$ cells, and total pulp cells were positive for CD29, CD44, CD90, and CD105 and negative for CD31 at the third passage, which are minimal criteria for MSCs. It is noteworthy that the percentages of pulp CD105$^+$ cells which expressed CD73, CD150, and CXCR4 were much higher compared with adipose CD105$^+$
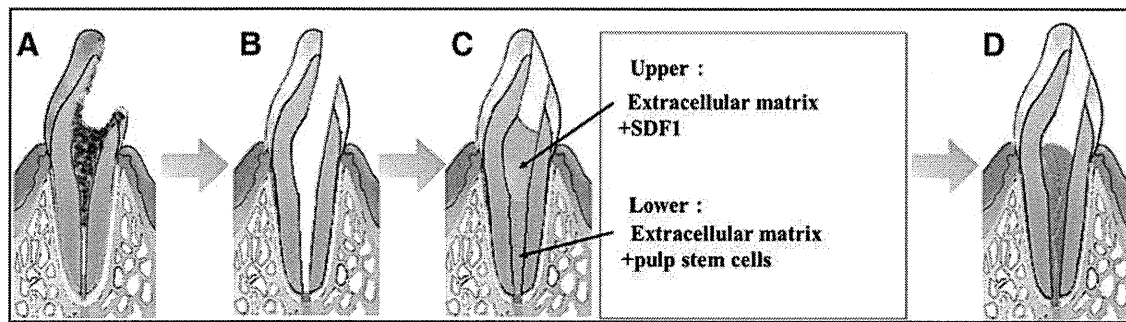
FIG. 4. Schematic diagrams of a canine model for complete pulp regeneration in permanent mature teeth. **(A)** pulpitis model, **(B)** whole pulp removal, and enlargement of apical foramen, 0.7 mm in width, **(C)** irrigation and filling with stem/ progenitor cells in the lower part and SDF-1 in the upper part of the root canal together with collagen scaffold, **(D)** complete pulp regeneration. Color images available online at www.liebertonline.com/tea

cells and total pulp cells (Table 1). The expression of stem cell markers, *CXCR4, Sox2, and Bmi1* mRNA, was 16.8, 64, and 3.5 times higher in pulp CD105$^+$ cells than those in total pulp cells, respectively, suggesting the stem cell properties of pulp CD105$^+$ cells. Further, the pulp-derived CD105$^+$ cells exhibited higher expression of the characteristic stem cell markers compared with the adipose-derived CD105$^+$ cells. Angiogenic factors and/or neurotrophic factors, *VEGF-A, GM-CSF, NGF, BDNF, neuropeptide Y, neurotrophin 3, E-selectin,* and *VCAM-1,* were expressed higher in pulp CD105$^+$ cells compared with total pulp cells and adipose CD105$^+$ cells (Fig. 2).

The differentiation of pulp CD105$^+$ cells into adipose cells (Fig. 3A, D), endothelial cells (Fig. 3E), neuronal cells (Fig. 3H, J, K), and odontoblast/osteoblast lineage (Fig. 3L, O) was observed. However, the mineralized matrix was higher in total pulp cells (Fig. 3M) than that in pulp CD105$^+$ cells (Fig. 3L). Adipose CD105$^+$ cells demonstrated adipogenic (Fig. 3C, D) and osteogenic potential (Fig. 3N, O) but neither angiogenic (Fig. 3G) nor neurogenic potential. The proliferation activity with SDF-1 was higher in pulp CD105$^+$ cells than that in total pulp cells and adipose CD105$^+$ cells (Fig. 3P). The migration activity with SDF-1 shown in the TAXIScan-FL was much higher in pulp CD105$^+$ cells compared with total pulp cells and adipose CD105$^+$ cells (Supplementary Videos A–C).

Pulp regeneration after transplantation of pulp CD105$^+$ cells in the root canal

We next demonstrated by the *in vivo* transplantation of autologous pulp CD105$^+$ cells with SDF-1 into the root canal of mature teeth induced complete apical closure after pulpectomy in dogs (Fig. 4). Pulp CD105$^+$ cells formed pulp-like tissue by day 14 when transplanted with SDF-1 (Fig. 5A–C). However, transplantation of CD105$^+$ cells alone (Fig. 5E), or SDF-1 alone (Fig. 5F), yielded less pulp. Statistical analysis showed that the regenerated area was significantly larger (3.3-fold and 4.2-fold increase) when pulp CD105$^+$ cells were transplanted with SDF-1 compared with CD105$^+$ cells alone or SDF-1 alone, respectively (Fig. 6). The odontoblast-like cells attached to the dentinal wall in the root canal, extending their processes into dentin tubules (Fig. 5D). The pulp-like tissue was further extended to the cementum-enamel junction under the cement filling 90 days after transplantation of pulp CD105$^+$ cells together with SDF-1 (Fig. 5G). The cells in the

upper part of the regenerated tissue were spindle shaped (Fig. 5H), and those in the middle part were stellate-like (Fig. 5I) similar to those in the normal pulp (Fig. 5J). It is noteworthy that tubular dentin was observed along the dentinal wall (Fig. 5G, K). The odontoblasts lining the dentinal wall were positive for *enamelysin/MMP-20* (Fig. 5L) and *Dspp* (Fig. 5M), two markers for odontoblasts. However, if unfractionated total pulp cells are transplanted instead of CD105$^+$ cells, less tissue was observed (Fig. 5N, O), followed by evidence of mineralization on day 90 (Fig. 5Q, R). Similarly, when adipose tissue-derived CD105$^+$ cells were transplanted, much less regenerate tissue was observed (Fig. 5P). Further statistical analysis showed that the ratio of newly regenerated tissue to root canal surface area was significantly larger (51.6-fold and 2.2-fold increase) in the case of pulp CD105$^+$ cell transplantation with SDF-1 than in the case of transplantation of adipose CD105$^+$ cells with SDF-1 or total pulp cells with SDF-1 on day 14 (Fig. 6). Confocal laser microscopic analysis after staining with BS-1 lectin of cryosections demonstrated neovascularization in the regenerated tissue (Fig. 7A). Two-photon microscopic analysis showed that numerous DiI-labeled transplanted pulp CD105$^+$ cells were in the vicinity of the newly formed capillaries (Fig. 7B), implicating a trophic role for these cells in neovascularization. The three-dimensional image of induced vascularization in the regenerated tissue on day 14 (Fig. 7D) was similar in density and orientation to that in the normal pulp (Fig. 7E). The transplanted CD105$^+$ cells were observed overall in the newly regenerated pulp (Fig. 7C), suggesting their potential capacity to migrate to the upper site by SDF-1. The neuronal process stained by PGP9.5 antibody was extended into the newly regenerated pulp from apical foramen (Fig. 7F). DiI labeling on the regenerated pulp in the lower third incisor *in vivo* showed the neuronal process from regenerated pulp connecting to inferior alveolar nerve (Fig. 7G).

Two-dimensional electrophoretic protein analyses and gene expression analyses of pulp regeneration

Two-dimensional electrophoretic analyses demonstrated that the qualitative and quantitative protein pattern of regenerated pulp tissue on day 28 was similar to that of normal pulp tissue derived from the same individual. The protein spots detected both in normal and regenerated pulp tissue represented 85.5% (123 spots) (Supplementary Fig. S1A–C). On the other hand, there were some differences in the protein

spots of normal pulp tissue compared with periodontal ligament (Supplementary Fig. S1D–F).

There have been no specific markers for pulp. Thus, some specific markers for periodontal ligament were used to further confirm normal pulp regeneration. Expression of
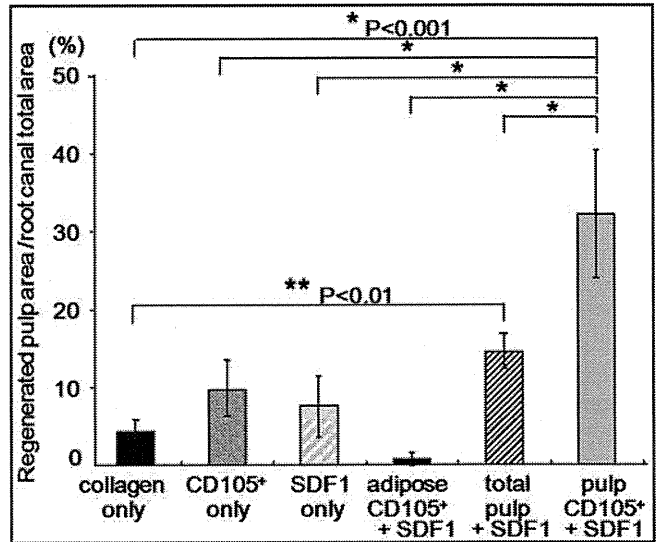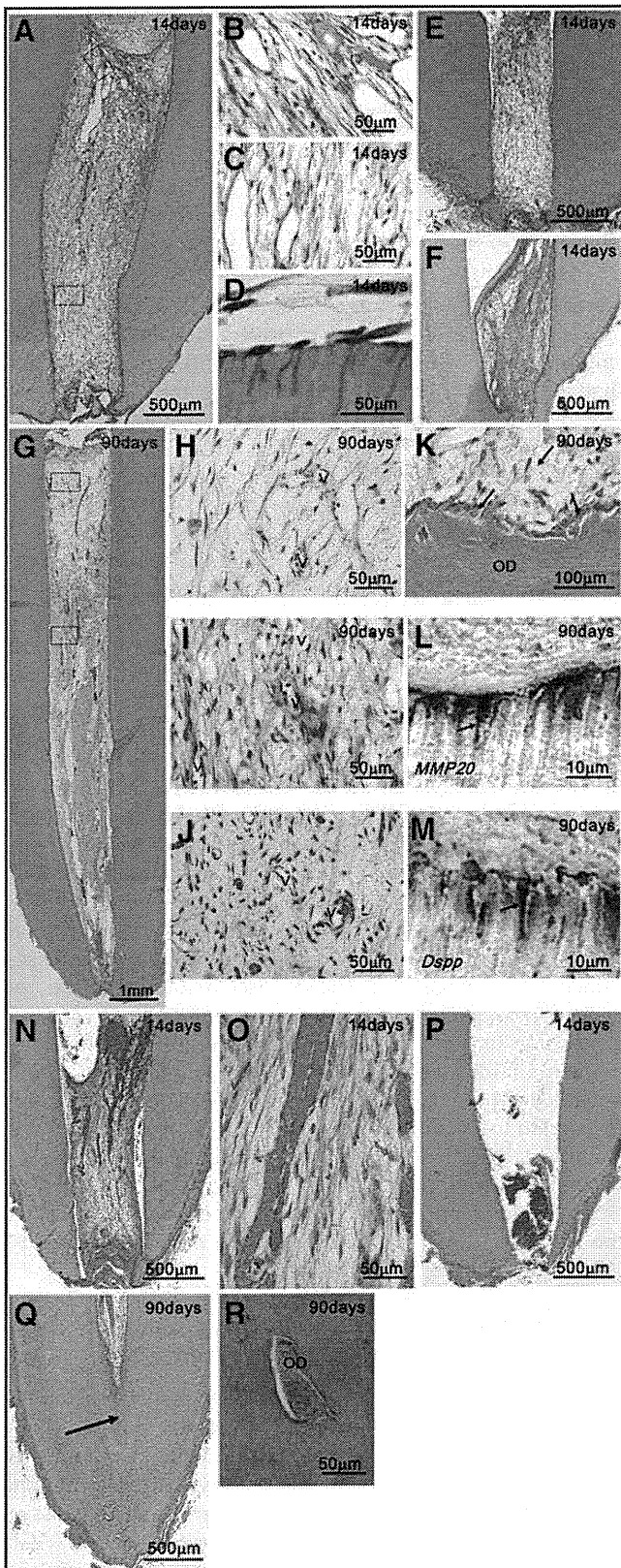

FIG. 6. Ratio of regenerated area to root canal area on day 14. Data are expressed as means ± standard deviation of five determinations. Statistical analysis was performed by the nonpaired Student's *t*-test.

axin2,[13] periostin,[14] and asporin/ PLAP-1[15] mRNA was much higher (25,531-fold, 179-fold, and 11-fold) in normal periodontal ligament than that in the regenerated tissue on day 28, respectively. Those genes were similarly expressed in a very low level in normal pulp compared with the regenerated tissue (0.4-fold, 0.4-fold, and 2.4-fold, respectively) (Fig. 8A). Collagen α*I*(*I*) was 9.3 times more expressed in periodontal ligament compared with the regenerated tissue, although this expression was not different between normal pulp and the regenerated tissue (Fig. 8A). Syndecan3 and TenascinC, known to be highly expressed in pulp,[16,17] were 14.3 times and 50.0 times more expressed in the regenerated tissue compared with periodontal ligament, although those expressions in the regenerated tissue were similar to those in normal pulp (Fig. 8B). Hierachical clustering based on Affymetrix data produced a clear pattern separation of normal pulp tissue and the regenerated tissue from periodontal ligament (Supplementary Fig. S1G). Thus, the two-dimensional

FIG. 5. Complete regeneration of pulp tissue after autologous transplantation of CD105^{+} cells with SDF-1 in the emptied root canal after pulpectomy in dogs. (A–F) Fourteen days after transplantation. (A–D) Pulp CD105^{+} cells with SDF-1. (E) Pulp CD105^{+} cells only. (F) SDF-1 only. (G–I, K–M) Ninety days after transplantation of pulp CD105^{+} cells with SDF-1. (H, I) Newly formed blood vessels (v) in the upper part and the middle part of regenerated tissue. (J) Normal pulp tissue. (K) Odontoblastic cells (arrows) lining to newly formed osteodentin/tubular dentin (OD) along with the dentinal wall. (L, M) In situ hybridization analyses of odontoblast differentiation (arrows). (L) Enamelysin/matrix metalloproteinase 20 (MMP-20). (M) Dentin sialophosphoprotein (Dspp). (N–P) Fourteen days after transplantation. (N, O) Total pulp cells with SDF-1. (P) Adipose-derived CD105^{+} cells with SDF-1. (Q, R) Ninety days after transplantation of total pulp cells with SDF-1. Mineralized tissue (arrow) and osteodentin (OD). Color images available online at www.liebertonline.com/tea
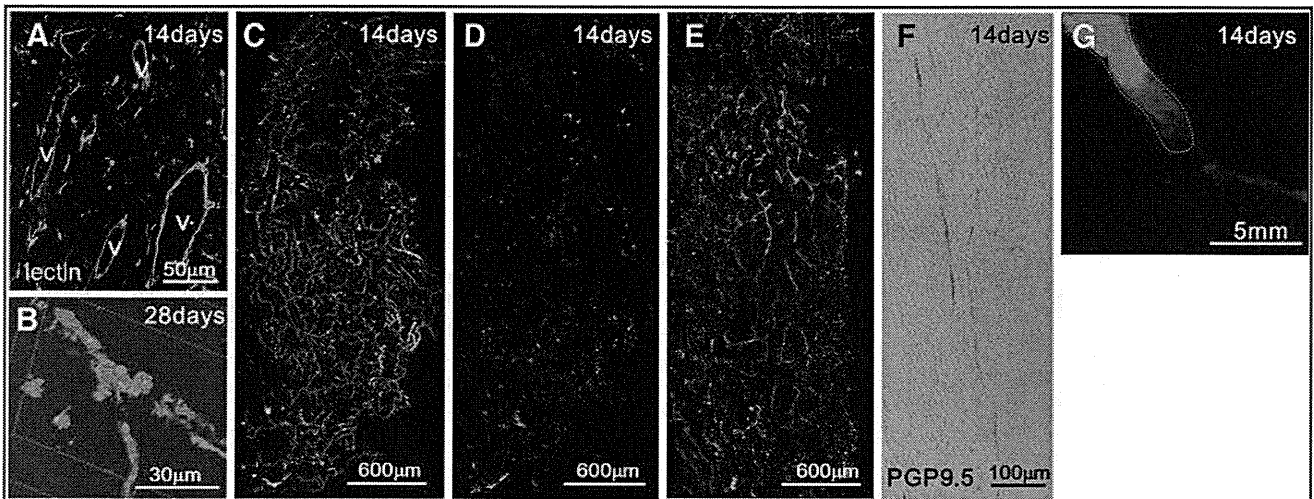
FIG. 7. (A) Immunostaining with BS-1 lectin. v: newly formed capillaries. (B–E) Three-dimensional images of new vascularization by whole mount immunostaining with lectin. (B) Note transplanted CD105^{+} cells in the vicinity of the newly formed capillaries. (D) The DiI labeled transplanted cells located overall in the tissue. (E) Normal pulp tissue. (F) Immunostaining with PGP 9.5. (G) Neurogenesis in newly formed pulp tissue (white dotted line) connecting to inferior alveolar nerve. Color images available online at www.liebertonline.com/tea

electrophoretic analyses and the gene expression analyses suggested that the regenerated pulp tissue was identical to true functional normal pulp.

Discussion

Regeneration of pulp tissue is an unmet need in endodontic therapy. The critical requirements for pulp regeneration are morphogenesis of pulp tissue replete with angiogenesis/vasculogenesis and neurogenesis.[3,18] The induction of pulp-like tissue has been reported in a tooth slice model of subcutaneous transplantation in immunodeficient mice, by filling of pulp stem cells and dentin matrix protein 1 (DMP1) together[19] or stem cells from exfoliated deciduous teeth only[20] in a thin tooth slice. Similarly, another model for the induction of pulp-like tissue was subcutaneous transplantation of human tooth root fragment (6–7 mm long) with

an enlarged root canal (1.0–1.25 mm in diameter) with one end sealed with mineral trioxide aggregate cement. Stem/progenitor cells from apical papilla and dental stem cells were inserted into the root. Pulp-like tissue with well-established vascularity and a continuous layer of odontoblast-like cells along the dentinal wall were observed as demonstrating the feasibility of pulp regeneration.[21] The novel finding in this investigation was the complete regeneration of whole pulp tissue after pulpectomy without tooth extraction by autologous pulp CD105^{+} cell transplantation with SDF-1 in mature teeth with complete apical closure.

Human pulp CD105^{+} cells have demonstrated angiogenesis/vasculogenic and neurogenic potential.[8] The SDF-1-CXCR4 axis plays a role in stem cell homing even in adulthood, especially after ischemia.[22] In this investigation, CXCR4 was highly expressed in canine pulp CD105^{+} cells. The regenerated pulp-like tissue was more in pulp CD105^{+}

FIG. 8. Relative mRNA expression of cytokines of markers for periodontal ligament (A), and for pulp (B) by real-time reverse transcription-polymerase chain reaction in regenerated pulp, normal pulp, and adipose periodontal tissue. The experiments were repeated four times, and one represented experiment is presented.
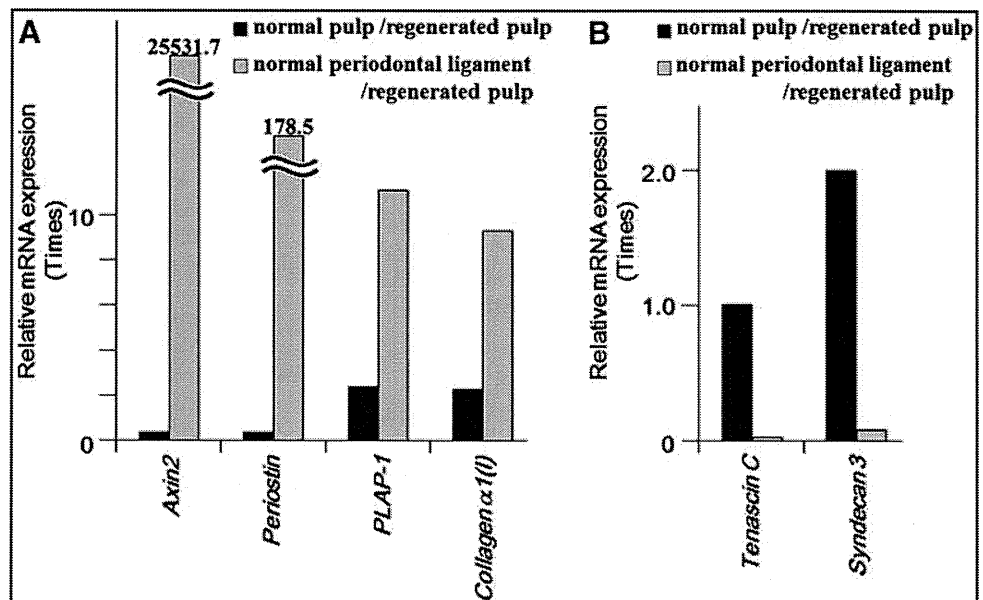
cells with SDF-1 compared with CD105$^+$ cells alone or SDF-1 alone. Therefore, these results suggested the combinatory effect of SDF-1 and pulp CD105$^+$ cells, especially SDF-1-CXCR4 axis for whole pulp regeneration. Similar contributions of SDF-1-CXCR4 axis, the 'homing' of stem cells expressing CXCR4 to a hypoxic-ischemic lesion where expression of SDF-1 significantly increased, have been reported in the rat ischemic brain after transplantation of human umbilical cord blood cells,[23] and in the myocardial ischemia,[24] or a subfraction of side population cells.[25]

Pulp tissue is readily available from discarded permanent teeth such as third molar and deciduous teeth after extraction. The autologous pulp stem cell source, however, is limited to patients who have discarded teeth with adequate pulp. Higher ratio of CD73 and CD150 positive cells and higher expression of CXCR4, Sox2, and Bmi1 mRNA is observed in pulp CD105$^+$ cells compared with adipose CD105$^+$ cells, suggesting more stemness of pulp CD105$^+$ cells. Higher angiogenic and neurogenic potential and higher expression of a variety of proangiogenic factors and neurotrophic factors in pulp CD105$^+$ cells is compared with adipose CD105$^+$ cells in vitro, and expression of cytokines VEGF-A and GM-CSF mRNA by the transplanted pulp stem cells in the vicinity of the newly formed vasculature in the regenerated pulp,[26] implying that the higher trophic actions of pulp CD105$^+$ cells on endothelial cells promote neovascularization. Thus, pulp CD105$^+$ cells are a more useful cell source in induction of pulp regeneration by cell therapy compared with adipose CD105$^+$ cells and total pulp cells.

The routine translation of the current findings to the clinic is dependent on the use of autologous pulp in normal healthy patients. However, in the aged and in patients with diabetes, the pulp tissue may be limiting and may require novel approaches.

Conclusion

Our data demonstrate for the first time that pulp CD105$^+$ cells with SDF-1 induce complete pulp regeneration replete with neurogenesis and vasculogenesis in vivo in the adult dog after experimental pulpectomy. This cell therapy demonstrates the potential clinical utility of fractionated CD105$^+$ cells for endodontic treatment for conservation of teeth in dentistry.

Acknowledgments

Disclosure Statement

The authors indicate no potential conflicts of interest.

References

1. Nakashima, M., and Akamine, A. The application of tissue engineering to regeneration of pulp and dentin in endodontics. J Endod 31, 711, 2005.

2. Nakashima, M., and Reddi, A.H. The application of bone morphogenetic proteins to dental tissue engineering. Nature Biotech 21, 1025, 2003.

3. Hargreaves, K.M., Giesler, T., Henry, M., and Wang, Y. Regeneration potential of the young permanent tooth: what does the future hold? J Endod 34, S51, 2008.

4. Huang, G.T. Apexification: the beginning of its end. Int Endod J 42, 855, 2009.

5. Barry, F.P., Boynton, R.E., Haynesworth, S., Murphy, J.M., and Zaia, J. The monoclonal antibody SH-2, raised against human mesenchymal stem cells, recognizes an epitope on endoglin (CD105). Biochem Biophys Res Commun 265, 134, 1999.

6. Wynn, R.F., Hart, C.A., Corradi-Perini, C., O'Neill, L., Evans, C.A., Wraith, J.E., Fairbairn, L.J., and Bellantuono, I. A small proportion of mesenchymal stem cells strongly expresses functionally active CXCR4 receptor capable of promoting migration to bone marrow. Blood 104, 2643, 2004.

7. Dar, A., Goichberg, P., Shinder, V., Kalinkovich, A., Kollet, O., Netzer, N., Margalit, R., Zsak, M., Nagler, A., Hardan, I., Resnick, I., Rot, A., and Lapidot, T. Chemokine receptor CXCR4-dependent internalization and resecretion of functional chemokine SDF-1 by bone marrow endothelial and stromal cells. Nat Immunol 6, 1038, 2005.

8. Nakashima, M., Iohara, K., and Sugiyama, M. Human dental pulp stem cells with highly angiogenic and neurogenic potential for possible use in pulp regeneration. Cytokine Growth Factor Rev 20, 435, 2009.

9. Lima e Silva, R., Shen, J., Hackett, S.F., Kachi, S., Akiyama, H., Kiuchi, K., Yokoi, K., Hatara, M.C., Lauer, T., Aslam, S., Gong, Y.Y., Xiao, W.H., Khu, N.H., Thut, C., and Campochiaro, P.A. The SDF-1/CXCR4 ligand/receptor pair is an important contributor to several types of ocular neovascularization. FASEB J 21, 3219, 2007.

10. van Weel, V., Seghers, L., de Vries, M.R., Kuiper, E.J., Schlingemann, R.O., Bajema, I.M., Lindeman, J.H., Delis-van Diemen, P.M., van Hinsbergh, V.W., van Bockel, JH., and Quax, P.H. Expression of vascular endothelial growth factor, stromal cell-derived factor-1, and CXCR4 in human limb muscle with acute and chronic ischemia. Arterioscler Thromb Vasc Biol 27, 1426, 2007.

11. Iohara, K., Zheng, L., Ito, M., Tomokiyo, A., Matsushita, K., and Nakashima, M. Side population cells isolated from porcine dental pulp tissue with self-renewal and multipotency for dentinogenesis, chondrogenesis, adipogenesis, and neurogenesis. Stem Cells 24, 2493, 2006.

12. Iohara, K., Zheng, L., Wake, H., Ito, M., Nabekura, J., Wakita, H., Nakamura, H., Into, T., Matsushita, K., and Nakashima, M. A novel stem cell source for vasculogenesis in ischemia: subfraction of side population cells from dental pulp. Stem Cells 26, 2408, 2008.

13. Lohi, M., Tucker, A.S., and Sharpe, P.T. Expression of Axin2 indicates a role for canonical Wnt signaling in development of the crown and root during pre- and postnatal tooth development. Dev Dyn 239, 160, 2010.

14. Suzuki, H., Amizuka, N., Kii, I., Kawano, Y., Nozawa-Inoue, K., Suzuki, A., Yoshie, H., Kudo, A., and Maeda, T. Immunohistochemical localization of periostin in tooth and its surrounding tissues in mouse mandibles during development. Anat Rec Part A 281, 1264, 2004.

15. Nakamura, S., Terashima, T., Yoshida, T., Iseki, S., Takano, Y., Ishikawa, I., and Shinomura, T. Identification of genes preferentially expressed in periodontal ligament: specific

expression of a novel secreted protein, FDC-SP. Biochem Biophys Res Commun **338**, 1197, 2005.

16. Hikake, T., Mori, T., Iseki, K., Hagino, S., Zhang, Y., Takagi, H., and Yokoya, S., Wanaka, A. Comparison of expression patterns between CREB family transcription factor OASIS and proteoglycan core protein genes during murine tooth development. Anat Embyol (Berl) **206**, 373, 2003.

17. Zhang, X., Schuppan, D., Becker, J., Reichart, P., and Gelderblom, H.R. Distribution of undulin, tenascin, and fibronectin in the human periodontal ligament and cementum: comparative immunoelectron microscopy with ultra-thin cryosections. J Histochem Cytochem **41**, 245, 1993.

18. Murray, PE, Garcia-Godoy, F., and Hargreaves, K.M. Regenerative endodontics: a review of current status and a call for action. J Endod **33**, 377, 2007.

19. Prescott, R.S., Alsanea, R., Fayad, M.I., Johnson, B.R., Wenckus, C.S., Hao, J., John, A.S., and George, A. *In vivo* generation of dental pulp-like tissue by using dental pulp stem cells, a collagen scaffold, and dentin matrix protein 1 after subcutaneous transplantation in mice. J Endod **34**, 421, 2008.

20. Cordeiro, M.M., Dong, Z., Kaneko, T., Zhang, Z., Miyazawa, M., Shi, S., Smith, A.J., and Nör, J.E. Dental pulp tissue engineering with stem cells from exfoliated deciduous teeth. J Endod **34**, 962, 2008.

21. Huang, G.T., Yamaza, T., Shea, L.D., Djouad, F., Kuhn, N.Z., Tuan, R.S., and Shi, S. Stem/progenitor cell-mediated *de novo* regeneration of dental pulp with newly deposited continuous layer of dentin in an *in vivo* model. Tissue Eng Part A **16**, 605, 2010.

22. Zaruba, M.M., and Franz, W.M. Role of the SDF-1-CXCR4 axis in stem cell-based therapies for ischemic cardiomyopathy. Expert Opin Biol Ther **10**, 321, 2010.

23. Rosenkranz, K., Kumbruch, S., Lebermann, K., Marschner, K., Jensen, A., Dermietzel, R., and Meier, C. The chemokine SDF-1/CXCL12 contributes to the 'homing' of umbilical cord blood cells to a hypoxic-ischemic lesion in the rat brain. J Neurosci Res **88**, 1223, 2010.

24. Wang, Y., Haider, H.Kh., Ahmad, N., Zhang, D., and Ashraf, M. Evidence for ischemia induced host-derived bone marrow cell mobilization into cardiac allografts. J Mol Cell Cardiol **41**, 478, 2006.

25. Liang, S.X., Tan, T.Y., Gaudry, L., and Chong, B. Differentiation and migration of Sca1 + /CD31- cardiac side population cells in a murine myocardial ischemic model. Int J Cardiol **138**, 40, 2010.

26. Iohara, K., Zheng, L., Ito, M., Ishizaka, R., Nakamura, H., Into, T., Matsushita, K., and Nakashima, M. Regeneration of dental pulp after pulpotomy by transplantation of CD31(-)/CD146(-) side population cells from a canine tooth. Regen Med **4**, 377, 2009.

Address correspondence to:
Misako Nakashima, Ph.D.
Department of Dental Regenerative Medicine
Center of Advanced Medicine for Dental and Oral Diseases
National Center for Geriatrics and Gerontology
Research Institute
35 Gengo, Morioka
Obu, Aichi 474-8522
Japan

E-mail: misako@ncgg.go.jp

This article has been cited by:

1. Ryo Ishizaka, Koichiro Iohara, Masashi Murakami, Osamu Fukuta, Misako Nakashima. 2011. Regeneration of dental pulp following pulpectomy by fractionated stem/progenitor cells from bone marrow and adipose tissue. *Biomaterials* . [CrossRef]
2. F.J. Rodríguez-Lozano, J.M. Moraleda. 2011. Use of dental stem cells in regenerative dentistry: A possible alternative. *Translational Research* . [CrossRef]

Dental Pulp-Derived CD31−/CD146−
Side Population Stem/Progenitor Cells Enhance
Recovery of Focal Cerebral Ischemia in Rats

Masahiko Sugiyama, D.D.S.,[1,2] Koichiro Iohara, Ph.D.,[1] Hideaki Wakita, Ph.D.,[3] Hisashi Hattori, Ph.D.,[2]
Minoru Ueda, Ph.D.,[2] Kenji Matsushita, Ph.D.,[1] and Misako Nakashima, Ph.D.[1]

Regenerative therapy using stem cells is a promising approach for the treatment of stroke. Recently, we reported that CD31−/CD146− side population (SP) cells from porcine dental pulp exhibit highly vasculogenic potential in hindlimb ischemia. In this study, we investigated the influence of CD31−/CD146− SP cells after transient middle cerebral artery occlusion (TMCAO). Adult male Sprague-Dawley rats were subjected to 2 h of TMCAO. Twenty-four hours after TMCAO, CD31−/CD146− SP cells were transplanted into the brain. Motor function and infarct volume were evaluated. Neurogenesis and vasculogenesis were determined with immunochemical markers, and the levels of neurotrophic factors were assayed with real-time reverse transcription–polymerase chain reaction. In the cell transplantation group, the number of doublecortin-positive cells increased twofold, and the number of NeuN-positive cells increased eightfold, as compared with the control phosphate-buffered saline group. The vascular endothelial growth factor level in the ischemic brain with transplanted cells was 28 times higher than that in the normal brain. In conclusion, CD31−/CD146− SP cells promoted migration and differentiation of the endogenous neuronal progenitor cells and induced vasculogenesis, and ameliorated ischemic brain injury after TMCAO.

Introduction

SEVERAL PRECLINICAL STUDIES have provided evidence that transplanted stem cells have therapeutic potential in the treatment of stroke.[1] Stem cells have the capability to migrate to areas of injury and secrete neuroprotective factors to induce neurogenesis.[2] In the adult mammalian brain, neurogenesis persists in certain distinct regions of the central nervous system such as the subventricular zone (SVZ) and the dentate gyrus of the hippocampus.[3] It has been reported that transplanting differentiated neural stem cells isolated from dental pulp improved motor disability and reduced infarct volume.[4] However, the influence of transplanting stem/progenitor cells isolated from dental pulp in cerebral ischemia has not been elucidated. Recently, we reported that CD31−/CD146− side population (SP) cells containing stem/progenitor cells from porcine dental pulp exhibit highly vasculogenic potential in vitro and promote revascularization in hindlimb ischemia.[5] In the present study, we investigated the effects of these cells on neurogenesis and vasculogenesis in a cerebral ischemia model in a rat. In addition, the effects on the motor dysfunction and infarct volume were evaluated after transient middle cerebral artery occlusion (TMCAO).

Materials and Methods

Isolation of CD31−/CD146− SP cells

CD31−/CD146− SP and CD31+/CD146− SP cells were isolated from porcine tooth germ, as described previously.[5] CD31−/CD146− SP cells were cultured in endothelial basal medium-2 (EBM-2, single quots cc–4176) with 10 ng/mL insulin-like growth factor 1 (IGF1), 10 ng/mL epidermal growth factor (EGF), and 10% fetal bovine serum (FBS). CD31+/CD146− SP cells were cultured in EBM-2 with 10 ng/mL bFGF, 10 ng/mL vascular endothelial growth factor (VEGF), 138 nM hydrocortisone, 0.09 mg/mL heparin, 50 μg/mL ascorbic acid, and 10% FBS. They were routinely subcultured up to 70% confluence under identical conditions.

Cerebral ischemia model

All animal experiments were approved by the Institutional Animal Care and Use Committee (National Center for the Geriatrics and Gerontology). Adult male Sprague-Dawley rats (Japan SLC, Inc.) weighing 300–400 g were used. Animals were initially anesthetized with 5% isoflurane (Abbott Laboratories) and maintained under anesthesia with 1.5% isoflurane in a mixture of 70% N_2O and 30% O_2. Rectal

temperature was maintained at 37°C±0.5°C on a heating pad. Focal cerebral ischemia was induced by TMCAO with 2 h.[6] A 4-0 monofilament nylon suture (Shirakawa) with the tip rounded by flame heating and silicone (KE-200; Shin-Etsu Chemical) was advanced from the external carotid artery into the internal carotid artery until it blocked the origin of the MCA. Two hours after occlusion, reperfusion was performed by withdrawal of the suture. The regional cerebral blood flow of the MCA territory was measured using a laser-Doppler flowmeter (Omega FLO-N1; Omega Wave, Inc.) after occlusion. The response was considered positive and included only if the reduction in regional cerebral blood flow was >70%.

Transplantation

Twenty-four hours after TMCAO (day 0), the rats were again anesthetized with sodium pentobarbital (Schering-Plough) (0.25 mL/kg, intraperitoneally) and maintained under anesthesia with 1.5% isoflurane in a mixture of 70% N_2O and 30% O_2. Animals were randomly divided into three groups: (I) $CD31^-/CD146^-$ SP cell transplantation group ($n = 24$, day 3 sacrificed = 6, day 9 sacrificed = 7, day 21 sacrificed = 11), (II) unfractionated pulp cell transplantation group ($n = 4$, used for motor function), and (III) vehicle alone (phosphate-buffered saline [PBS]) group ($n = 20$, day 3 sacrificed = 6, day 9 sacrificed = 5, day 21 sacrificed = 9). The infarction site was targeted for transplantation at the striatum of the following coordinates: 1.0 mm rostral to the bregma, 6.0 mm lateral to the midline, 5.0 mm ventral to the dura (Fig. 1A, B). Subsequently, 1×10^6 $CD31^-/CD146^-$ SP cells or unfractionated pulp cells at the fifth to seventh passage after labeling with 1,1-dioctadecyl-3,3,3,3 tetramethylindocarbocyanine perchlorate (DiI; Sigma), and removing all added factors into each medium were diluted with 2 μL of PBS, and were transplanted by Hamilton micro-syringe (Hamilton). The control group consisted of an equal volume of PBS injected into the same site.

Immunohistochemistry

At day 3 or 21 after injection, the rat was transcardially perfused with 4% paraformaldehyde solution (Nakarai Tes-que). The brain was removed and postfixed in paraformal-dehyde. The following day, it was immersed in 30% sucrose solution. Twelve-micrometer-thick coronal sections were cut on a cryostat. For immunohistochemistry, the sections were preincubated in blocking solution (PBS containing 5% normal serum of the species in which the secondary antibody was raised) for 2 h at room temperature, and incubated with primary antibodies diluted for 1 h at room temperature. The primary antibodies were as follows: neuronal progenitor cells (NPC) marker, rabbit anti-doublecortin (1:50; Abcam, Inc.); neuron marker, rabbit anti-neurofilament H (1:200; Chemicon) and mouse anti-NeuN (anti-neuronal nuclei, 1:500; Chemicon); endothelial cell marker, mouse anti-RECA1 (rat endothelial cell antigen; Monosan); apoptosis marker, rabbit anti-cleaved caspase-3 (1:50; Cell Signaling Technology, Inc.); and VEGF marker, rabbit anti-VEGF (VEGF [P-20]: sc-1836; Santa Cruz Biotech). After washing, sections were incubated for 1 h at room temperature with secondary antibodies (on day 21, for neurofilament H/dou-blecortin, Donkey anti-rabbit IgG FITC [1:400; Jackson Im-munoResearch]; for NeuN/RECA1, Goat anti-mouse IgG FITC [1:200; MP Biomedicals]; and for VEGF, rabbit anti-goat
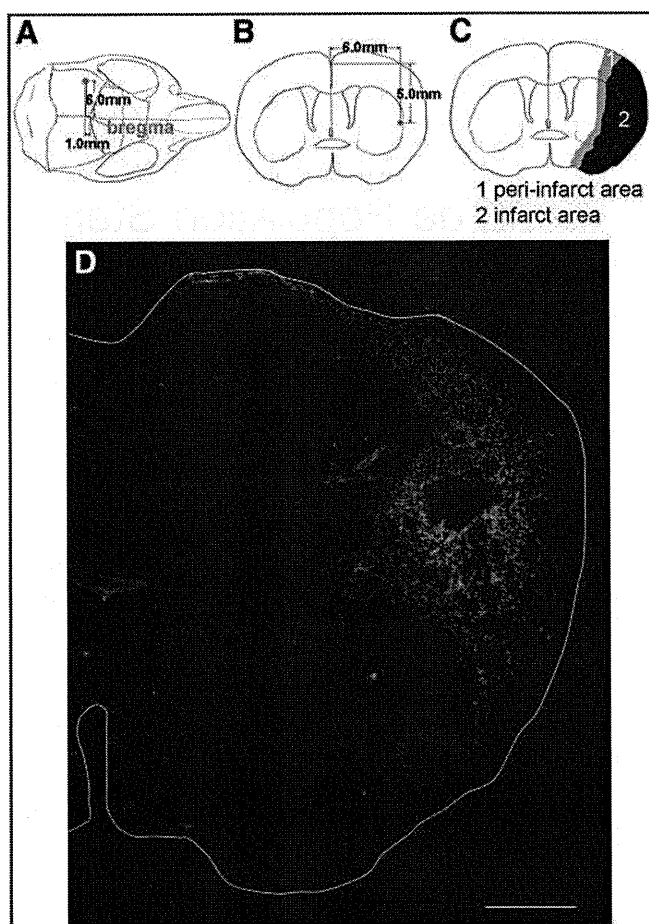

FIG. 1. **(A)** Overhead and **(B)** coronal view of the injection site. **(C)** The peri-infarct area. Peri-infarct area (gray), infarct core (black). **(D)** DiI-labeled transplanted $CD31^-/CD146^-$ SP cells (red) migrated from the original injection site to the peri-infarct area in the cortex and striatum. White outline is the outer circumference of brain. Scale bar = 1000 μm. SP, side population. DiI, 1,1-dioctadecyl-3,3,3,3 tetramethylindo-carbocyanine perchlorate. Color images available online at www.liebertonline.com/tea

IgG-HRP [1:400; Invitrogen Corporation]. On day 3, for cleaved caspase-3, goat anti-rabbit IgG-HRP [1:400; Invitro-gen] and for VEGF, rabbit anti-goat IgG-HRP [1:400; In-vitrogen]). The sections with HRP-conjugated secondary antibodies were incubated in anti-fluorescein-HRP (1:400; TSA™ Fluorescence Systems; PerkinElmer) for 7 min at room temperature. Adjacent sections were used as negative controls. In the control sections, all procedures were processed in the same manner except that the primary antibodies were omitted. To identify migration of NPC from SVZ, we observed the cryosections on days 9 and 21 with anti-doublecortin on fluorescence microscope (BZ-9000; Keyence) and BZ-HIC (Keyence).

Statistical analyses of the density of cells

The density of NPCs, neurons, endothelial cells, and apoptotic cells in the peri-infarct area (Fig. 1C) and the contralateral region in the $CD31^-/CD146^-$ SP cell transplantation group and PBS groups were determined. In all groups (PBS group, $CD31^-/CD146^-$ SP cell transplantation group,

TABLE 1. PORCINE PRIMERS FOR REAL-TIME REVERSE TRANSCRIPTION–POLYMERASE CHAIN REACTION AND *IN SITU* HYBRIDIZATION

Gene		5' DNA sequence 3'	Product size (bp)	Accession no.
r.β-actin	Forward	AAGTACCCCATTGAACACGG	257	NM_031144
	Reverse	ATCACAATGCCAGTGGTACG		
p.β-actin	Forward	CTGGGGCCTAACGTTCTCAC	198	BI118314
	Reverse	GTCCTTTCTTCCCCGATGTT		
VEGF	Forward	ATGGCAGAAGGAGACCAGAA	224	MN_214084
	Reverse	ATGGCGATGTTGAACTCCTA		
BDNF	Forward	TTCAAGAGGCCTGACATCGT	180	MN_214259
	Reverse	AGAAGAGGAGGCTCCAAAGG		
NGF	Forward	TGGTGTTGGGAGAGGTGAAT	210	L31889
	Reverse	CCGTGTCGATTCGGATAAA		
GDNF	Forward	ACGGCCATACACCTCAATGT	144	GU229658
	Reverse	CCGTCTGTTTTTGGACAGGT		

BDNF, brain-derived neurotrophic factor; GDNF, glial cell line-derived neurotrophic factor; NGF, nerve growth factor; VEGF, vascular endothelial growth factor.

and contralateral group, $n=3$), each five sections at every 120-μm were stained with doublecortin, NeuN, RECA1, and cleaved caspase-3. The microscopic images were scanned and five typical frames ($0.49\,mm^2$) were measured for each section. Thus, 75 frames on an average were determined per group. The positively stained area relative to total area ($7.41\,mm^2$) was statistically analyzed using a Dynamic cell count, BZ-HIC (Keyence).

Real-time reverse transcription–polymerase chain reaction

Total RNA on cryosamples was extracted using Trizol (Invitrogen) from the area of the DiI-positive cells observed in the section. First-strand cDNA syntheses were performed from total RNA by reverse transcription with ReverTra Ace-α (Toyobo). Real-time reverse transcription–polymerase chain reaction (RT-PCR) amplifications were performed at 95°C for 10 s, at 62°C for 15 s, and at 72°C for 8 s using the porcine-specific primers VEGF. The specificity of the primers to porcine was confirmed by no amplification of the first-strand cDNA from rats with normal brains. The RT-PCR products were subcloned into a pGEM-T Easy vector (Promega) and confirmed by DNA sequencing based on published cDNA sequences. Gene expression of the transplanted cells in the infarct area was compared with that in the porcine normal brain tissue and that in transplanted cells in the normal brain after normalizing with β-actin.

In situ *hybridization*

Neurotrophic factors expressed in CD31$^-$/CD146$^-$ SP cells were examined with *in situ* hybridization in cryosections on day 21. Porcine cDNA of VEGF (224 bp), glial cell line-derived neurotrophic factor (*GDNF*; 144 bp), brain-derived neurotrophic factor (*BDNF*;180 bp), and nerve growth factor (*NGF*; 210 bp) were linearized with NcoI, SpeI, NcoI, and SpeI, respectively, for anti-sense probes, and linearized with SpeI, NcoI, SpeI, and NcoI, respectively, for sense probes. The VEGF probe was constructed from plasmids after subcloning the PCR products using the same primers designed for real-time RT-PCR. The GDNF, BDNF, and NGF probes were also constructed in same way as the VEGF probe. Since

a published porcine GDNF sequence was not available, human primers for GDNF (forward 5'-TATGGGATGTCGT GGCTGT-3', reverse 5'-TCCACACCTTTTAGCGGAAT-3') were used for cDNA subcloning of porcine GDNF (630 bp). The design of the oligonucleotide primers (Table 1) was based on both published porcine cDNA sequences and the newly cloned cDNA sequence of the porcine GDNF. The four probes were labeled with DIG (Invitrogen) and the DIG signals were detected with TSA system FITC-conjugated tyramide (Invitrogen).

Migration, proliferation, and anti-apoptotic assays

At 50% confluence, the culture medium was switched to serum-free EBM-2. The conditioned medium (CM) from CD31$^-$/CD146$^-$ SP cells, CD31$^+$/CD146$^-$ SP cells, and unfractionated pulp cells were collected after 48 h.

For migration assay, modified Boyden chamber assays were performed with polyethylene terephthalate membrane (BD Bioscience) in a 24-well plate (BD Bioscience). SHSY5Y cells (Sanyo Chemical Industries, Ltd.) (1×10^5 cells/well) were seeded on the insert polyethylene terephthalate membrane, and 500 μL of DMEM-F12 (Sigma) with 20% of the three CMs was, respectively, poured into the tissue culture 24-well plate. SHSY5Y cells were derived from a neural crest tumor of early childhood, predominantly composed of un-differentiated neuroblast-like cells.[7] After 24 h, the SHSY5Y cells passing through the membrane were counted after detaching them with 0.05% trypsin–0.02% EDTA.

For cell proliferation assay, SHSY5Y cells (1×10^3/96-well plate) were cultured in DMEM-F12 containing 10% FBS for 24 h, and subsequently in serum-free DMEM-F12 containing 0.2% bovine serum albumin for further 24 h. Then, the medium was changed into each DMEM-F12 containing 0.02% FBS with 20% of three CMs. Ten micrometers of Tetra-color one (Seikagaku Kogyo, Co.) was added to the 96 well-plate, and cell numbers were measured by spectrophotometry at 450 nm at 2, 12, 24, 36, and 48 h of culture.

For the anti-apoptotic assay, SHSY5Y cells were cultured in DMEM-F12 in a 35-mm dish for 2 days and then incubated with 300 nM staurosporine[8] (Sigma) in DMEM-F12 with 20% of the three CMs. After 24 h, SHSY5Y were harvested, and

the cell suspensions were treated with Annexin V-FITC (Roche Diagnostics) and PI for 15 min, and analyzed by flow cytometry JSAN.

BDNF (Peprotech), GDNF (Peprotech), VEGF-A (Peprotech), or NGF (Peprotech) at 50 ng/mL was used as a control for the three assays.

Evaluation of motor disability

Rats were blindly examined on days 0, 2, 6, and 9 with a standardized motor disability scale by slight modifications.[9] Rats were scored 1 point for each of the following parameters: flexion of the forelimb contralateral to the stroke when instantly hung by the tail, extension of the contralateral hind limb when pulled from the table, and rotation to the paretic side against resistance. In addition, 1 point was scored for circling motion to the paretic side when trying to walk, 1 point was scored for failure to walk out of a circle of 50 cm in diameter within 10 s, 2 points were scored for failure to leave the circle within 20 s, and 3 points were scored for inability to exit the circle within 60 s. In addition, 1 point each was

scored for inability of the rat to extend the paretic forepaw when pushed against the table from above, laterally, and sideways. The motor disability scale was performed 3 times per animal time-point.

Assessment of infarct volume

The cryosections obtained from samples on days 3 and 21 were stained with hematoxylin and eosin.[10] ImageJ (National Institutes of Health) was used to determine each infarct area in 9 coronal sections in 12-μm thickness at 0.84-mm intervals. All of the infarction area was covered by these nine coronal sections. Regional infarct volumes were calculated by summing the infarct areas and multiplying these areas by the distance between sections (0.84 mm), followed by remediation for brain edema.[11]

Statistical analyses

Data are reported as means ± SD. p-Values were calculated using the unpaired Student's t-test.

FIG. 2. Doublecortin-positive cells (green: A–C), Neurofilament-positive cells (green: D–F), and NeuN-positive cells (green: G–I). CD31⁻/CD146⁻ SP cells (red) transplantation group of the ipsilateral (A, D, G) and the contralateral (B, E, H) on day 21. PBS group (C, F, I) on day 21. Statistical analyses of density of NPCs (J) and neurons (K) on day 21. Scale bars = 20 μm. *p < 0.005, **p < 0.001, Student's t-test. Each point is expressed as mean ± SD of 75 determinations. NPC, neuronal progenitor cells; PBS, phosphate-buffered saline. Color images available online at www.liebertonline.com/tea
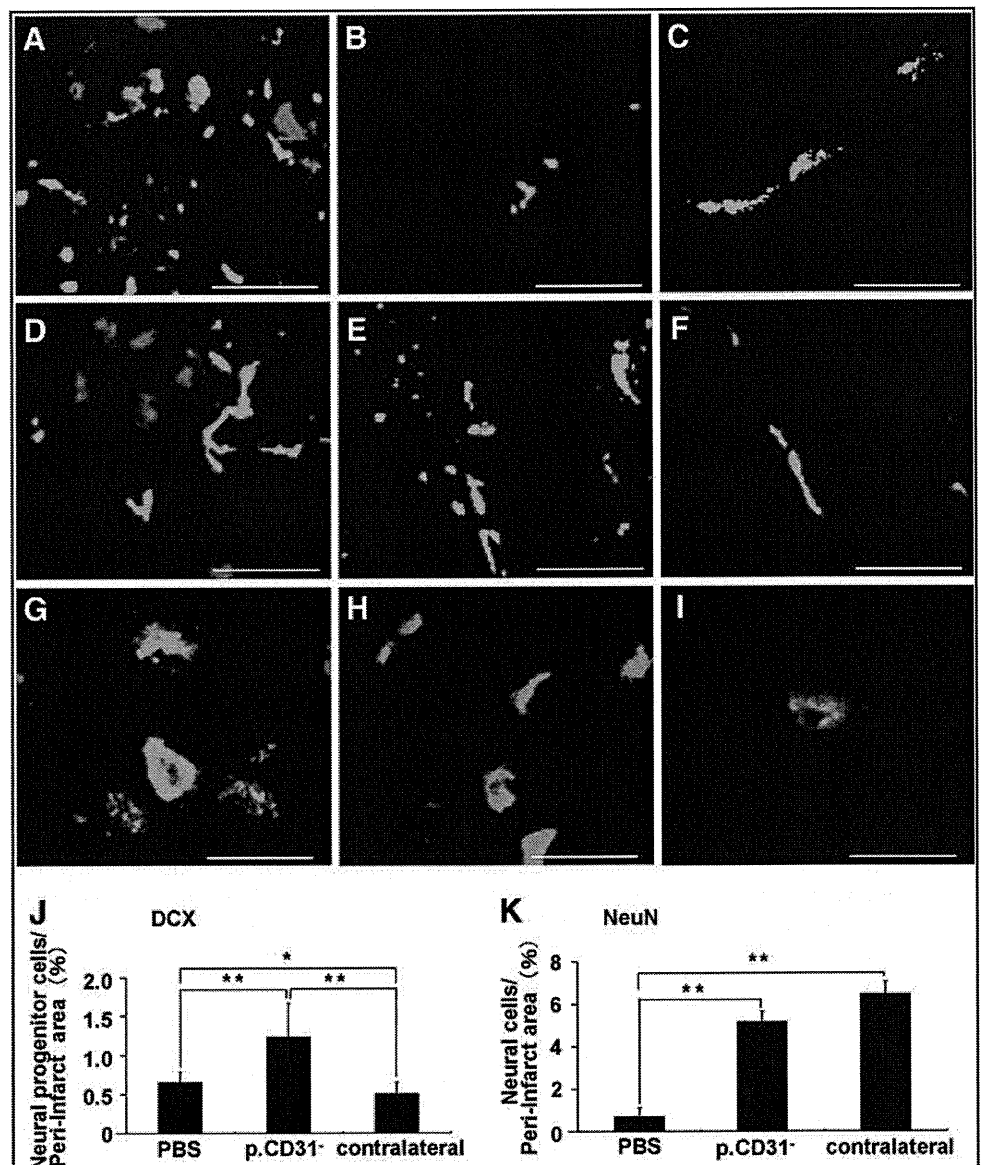
Results

Pulp stem cell outcome

DiI-labeled transplanted CD31⁻/CD146⁻ SP cells were characterized by round-to-oval nuclei with minimal variable cytoplasm. The transplanted cells survived and migrated from the original injection site to peri-infarct area in the cortex and striatum (Fig. 1D).

Transplanted cells localized in proximity of doublecortin (Fig. 2A) and neurofilament (Fig. 2D) or NeuN-positive cells (Fig. 2G) on day 21. Few doublecortin cells were observed in the contralateral side (Fig. 2B). There was a twofold increase in doublecortin-positive cells (Fig. 2J) and an eightfold increase in NeuN-positive cells (Fig. 2K) on day 21 in the CD31⁻/CD146⁻ SP cell transplantation group compared with that in the PBS group. No evidence of differentiation of CD31⁻/CD146⁻ SP cells into neurons or endothelial cells was detected. The migration of NPCs with doublecortin from SVZ to the peri-infarct area was observed on days 9 and 21. The migration on day 9 was more prominent (Fig. 3I, K, M). These results suggest that the transplanted cells support the migration and differentiation of the NPCs. The number of
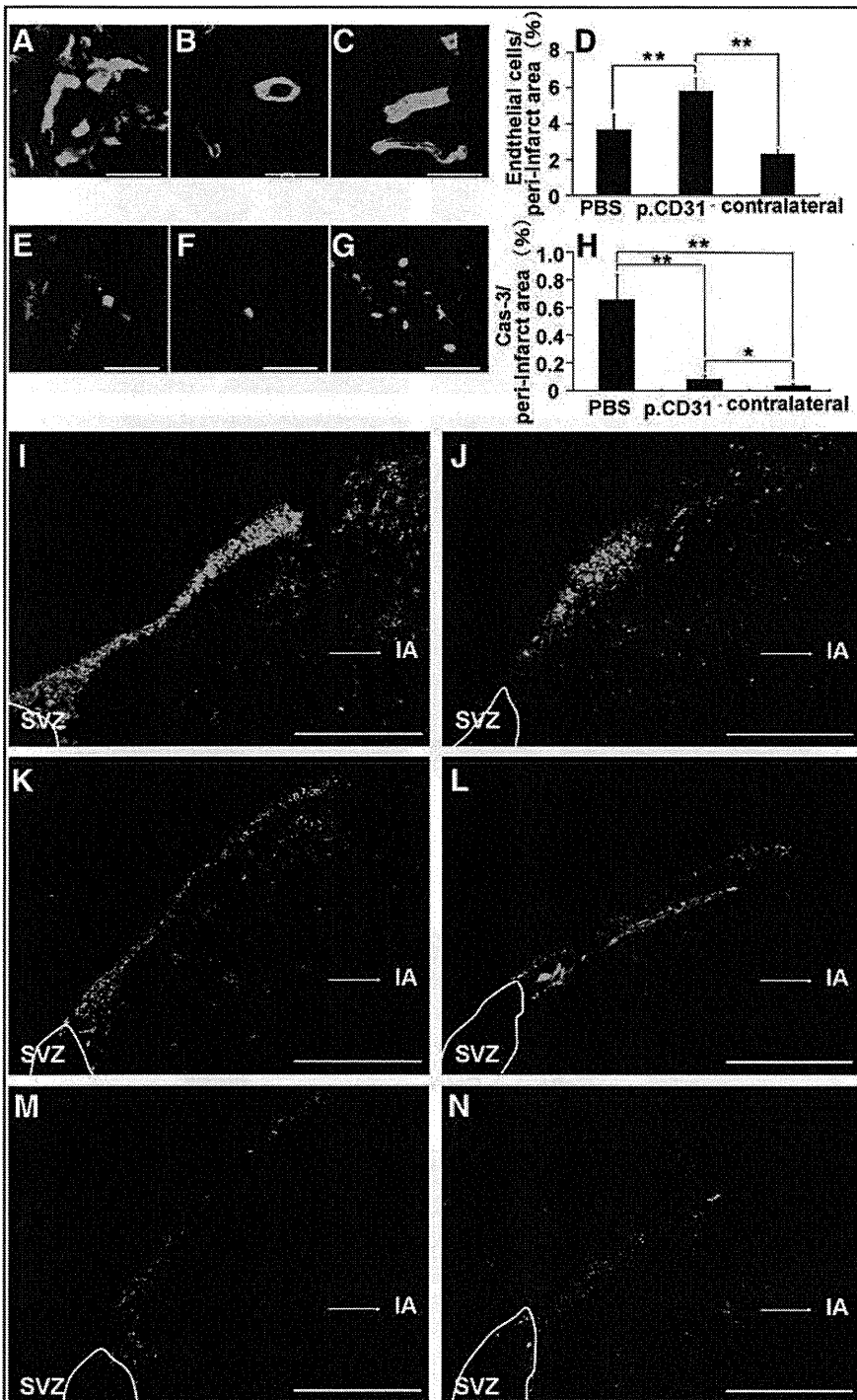

FIG. 3. RECA1-positive cells on day 21 (green: A–C) and cleaved caspase-3-positive cells on day 3 (green: E–G). CD31⁻/CD146⁻ SP cells (red) transplantation group of the ipsilateral (A, E) and the contralateral (B, F). PBS group (C, G). Statistical analyses of density of endothelial cells on day 21 (D) and cleaved caspase-3-positive cell on day 3 (H). The migration of NPC from the SVZ to the peri-infarct area on days 9 (I, J, M) and 21 (K, L, N). CD31⁻/CD146⁻ SP cells group (I, J). Unfractionated pulp cells (K, L). PBS group (M, N). Scale bar=20 μm (A–C, E–G), and 300 μm (I–N). *$p < 0.01$, **$p < 0.001$, Data were expressed as means±SD at 75 determinations. The statistical difference was calculated by Student's t-test. IA, infarct area; SVZ, subventricular zone. Color images available online at www.liebertonline.com/tea